Generic methodology for calibrating profiling nacelle lidars

Borraccino, Antoine; Courtney, Michael; Wagner, Rozenn

Publication date:
2015

Document Version
Publisher's PDF, also known as Version of record

UniTTe

Innovation Fund Denmark
RESEARCH, TECHNOLOGY & GROWTH

DTU

Generic methodology for calibrating profiling nacelle lidars

DTU Wind Energy E-Report-0086

A. Borraccino, M. Courtney, R. Wagner

DTU Wind Energy E-0086

July 2015

DTU Wind Energy
Department of Wind Energy

Author(s): A. Borraccino, M. Courtney, R. Wagner

Title: Generic methodology for calibrating profiling nacelle lidars

Department: DTU Wind Energy

Abstract:
Improving power performance assessment by measuring at different heights has been demonstrated using ground-based profiling LIDARs. More recently, nacelle-mounted lidars studies have shown promising capabilities to assess power performance. Using nacelle lidars avoids the erection of expensive meteorology masts, especially offshore. A new generation of commercially developed profiling nacelle lidars has sophisticated measurement capabilities.

As for any other measuring system, lidars measurements have uncertainties. Their estimation is the ultimate goal of a calibration. Field calibration procedures have been developed for non-profiling nacelle lidars. However, their specificity to one type of lidar or another highlights the need for developing generic calibration procedures. Such procedures should be applicable to any type of existing and upcoming lidar technology.

Profiling nacelle lidars, either scanning or featuring a multiple number of beams, measure parameters such as wind speed and direction, shear, veer, etc. The wind parameters are reconstructed combining line-of-sight velocity measurements – also called radial wind speed. In the generic calibration procedure, the radial wind speed is calibrated rather than a reconstructed parameter.

This contribution presents a generic methodology to calibrate profiling nacelle-mounted lidars. The application of profiling lidars to wind turbine power performance and corresponding need for calibration procedures is introduced in relation to metrological standards. Further, two different calibration procedure concepts are described along with their strengths and weaknesses. The main steps of the generic methodology are then explained and illustrated by calibration results from two types of profiling lidars. Finally, measurement uncertainty assessment methodologies are explored and the corresponding results discussed.

DTU Wind Energy E-0086

July 2015

ISBN: 978-87-93278-36-3

Contract no.: InnovationsFondens 1305-00024B

Project: UniTTe
http://www.unitte.dk/

Funding:
Innovation Fund Denmark

Pages: 60
Tables: 11
Figures: 22
References: 16

Technical University of Denmark
DTU Wind Energy
Risø Campus
Frederiksborgvej 399
DK-4000 Roskilde
Denmark

www.vindenergi.dtu.dk

Table of contents

Figures and tables

Nomenclature

a.g.l.: above ground level
CNR: carrier-to-noise ratio
CW: continuous wave
DK: Denmark
GPS: global positioning system
GUM: Guide to the expression of uncertainty in measurement [7]
HWS: horizontal wind speed
IEC: the International Electrotechnical Commission
LiDAR: light detection and Ranging
LOS: line-of-sight
RSS: residual sum of squares
RWS: radial wind speed
SI: International System of unis
SSR: sum of squares of residuals
VIM: International vocabulary of metrology [6]
WD: wind direction
ZDM: ZephIR Dual-Mode lidar

$\langle \ \rangle$: scalar time average
$\langle \ \rangle_{\mathrm{vec}}$: vector time average
$stdv$: standard deviation
cov: covariance
$r(x, y)$: cross-correlation coefficient between x and y

α: cone or half-opening angle
α_{exp}: shear exponent of the assumed wind profile
c : speed of light
c_{air}: speed of light in air
δv: Doppler frequency shift
ΔRWS: lidar measurement error vs. reference instrument
θ: wind direction
θ_0: estimation of LOS_{dir}
θ_{proj}: projection angle used to evaluate LOS_{dir}
λ: laser light wavelength
v: laser light frequency
σ_X: standard deviation of X
φ: tilt inclination angle (lidar indicated)
$\varphi_{physical}$: physical inclination of a lidar beam
$\varphi_{indicated}$: lidar indicated tilt inclination angle
φ_{BE}: best estimate of the lidar tilt inclination angle
a_{tilt}, b_{tilt}: gain and offset of the unforced linear regression on the tilt inclinometer
a_{roll}, b_{roll}: gain and offset of the unforced linear regression on the roll inclinometer
D_{config}: lidar measurement range to configure
D_{rotor}: rotor diameter of a wind turbine
$D_{physical}$: physical distance
D_{probe}: probe length
f_{fit}: fitting function
H_{lidar}: height of lidar a.g.l.
H_{mast}: height of meteorology mast a.g.l.
HWS_{proj}: projection of horizontal wind speed
k: coverage factor
LOS_{dir}: line-of-sight direction
n_i: number of points in bin i
n_{medium}: refraction index in specified medium
$Ref_{eq\ RWS}$: reference equivalent radial wind speed
RWS_{BE}: best estimate of lidar RWS
$RWS_{indicated}$: lidar indicated RWS (raw, uncorrected)
RWS_{norm}: normalised radial wind speed
u_c: combined uncertainty
u_{cal}: calibration uncertainty of cup anemometer HWS
u_{ope}: operational uncertainty of cup anemometer HWS
u_{mast}: mounting uncertainty of reference instrument on mast
u_{WD}: wind direction uncertainty
$u_{LOS\ dir}$: LOS direction uncertainty
u_{φ}: physical tilt inclination angle uncertainty
u_{pos}: positioning uncertainty
u_H: height uncertainty
u_{range}: lidar measurement range uncertainty
u_{inc}: inclined beam uncertainty
U_X: expanded uncertainty of X
u : streamwise component of the horizontal wind speed vector
v: spanwise component of the horizontal wind speed vector
V_{LOS}: line-of-sight velocity
X_i: value of X in bin number i
y_m: estimated measurand of the RWS

Preface

This report describes a generic calibration methodology for profiling nacelle-mounted lidars. The procedures have been developed as part of work package 2 of the Unified Turbine Testing project (UniTTe, http://www.unitte.dk/) funded by *Innovation Fund Denmark*. The report is deliverable D.2.1. Two lidars of the UniTTe project have been calibrated according to the generic methodology. Subsequently, two calibration reports specific to each lidar will be delivered (deliverables D.2.2 and D.2.3).

Antoine Borraccino
Ph.d.-student

Acknowledgements

I would first like to thank M. Courtney and R. Wagner who guided the work performed and reported in this document. This report really builds on the experience gained in the past by M. Courtney and the whole TEM section at DTU Wind Energy in calibrating ground-based, nacelle-based or even scanning lidars.

Thanks also to M. Harris, C. Slinger (ZephIR Lidar) and M. Boquet (Avent Lidar Technology) for their support in this project. Thanks finally to S.A. Sørensen (DTU-TEM's database engineer) for answering all my data requests and to all DTU Wind Energy technicians who helped us developing the calibration procedures and setting up the measurement campaigns, particularly A. Ramsing Vestergaard, K. Schrøder and P. Hansen.

Chapter 1

1 Introduction

1.1 Use of profiling lidars for power performance assessment

In recent years, the rapid increase in wind turbines size has created a need for developing new power performance assessment procedures. The effects of wind speed and direction variations over the rotor swept area on power curves can no longer be neglected [1]. Measuring the wind in one point, e.g. hub height, has consequently become insufficient.

Light detection and ranging (lidar) is a remote sensing technology addressing this challenge. Its multiple applications have found their way into the wind energy market. Ground based lidars are presently being used to measure wind profiles. They offer a practical and accurate solution for measuring wind over the entire rotor disk. On the other hand, even though two-beam nacelle lidars completing horizontal wind speed measurements are unable to measure the wind shear, they show promising capabilities to assess power performance [2] and avoid the erection of expensive meteorology masts, especially offshore. A new generation of commercially developed profiling nacelle lidars combine the benefits of both.

A wind profiling nacelle lidar measures the wind at multiple heights upstream of a turbine and from its nacelle – or downstream for wake measurements. The commercially available technology ranges from scanning lidars to multi-beam systems, e.g. the Zephir Dual-Mode (ZDM; circular scanning pattern) and the 5-beam Avent Demonstrator lidar (Figure 1).

Figure 1. Wind profiling lidar examples: 5-beam AventLidar Demonstrator (left) and ZephIR DM (right)

The next generation of standards for power performance testing is likely to include profiling nacelle lidars. In that context, the measurement uncertainties of such lidars must be estimated.

1.2 Levels of measurand in a lidar

Understanding the basic principles of lidars is essential in order to develop adequate calibration procedures. A lidar probes the wind by emitting light through a laser beam and at a known frequency. Aerosols, contained in the atmosphere and moving with the wind, scatter part of the laser light back to the lidar. The frequency of the backscattered light is slightly shifted due to the Doppler effect.

Profiling nacelle lidars feature a pre-defined scanning pattern. Continuous wave (CW) lidars probe the wind by scanning continuously, e.g. circularly using a prism to orient the laser beam. Pulsed lidars most commonly use discrete beams, e.g. five beams in a square pattern (4 corners + centre). Thus, for both CW and pulsed lidars, the beams are oriented in different directions in space, with an angle from the optical centreline of the lidar. Additionally, lidars can measure at several ranges.

One can distinguish different levels of measurands (in bold) – i.e. a quantity intended to be measured, from raw signal to end-user data:

- The "rawest" measurand is the **electrical current** generated by the lidar's photodiode as a result of the impinging backscattered light.
- The Doppler spectra obtained by performing spectral analysis on the signal (e.g. Fast Fourier Transform). The measurand at this level is the **distribution of Doppler frequency shifts**[1].
- The **Doppler frequency shift $\boldsymbol{\delta\nu}$** estimated from the Doppler spectra, using an estimator algorithm (e.g. centroid, peak or maximum likelihood).
- The **Radial Wind Speed** (RWS) also called line-of-sight (LOS) wind velocity and denoted V_{LOS} is directly proportional to the Doppler frequency shift:

$$V_{LOS} = \frac{\delta\nu \cdot \lambda}{2} = \frac{\delta\nu}{2} \cdot \frac{c}{\nu} \qquad \text{(eq. 1)}$$

  where $c = 2.998 \cdot 10^8\ m.s^{-1}$ is the speed of light in vacuum, λ is the laser light wavelength[2] and ν the corresponding frequency (usually $\lambda \sim 1.56\ \mu m$).
  The RWS is the projection of the wind vector onto the LOS.
- **Reconstructed wind parameters**: RWS measurements are combined and assumptions usually made – e.g. horizontal flow homogeneity – to reconstruct wind parameters. For example, profiling lidars reconstruction algorithms can derive wind speed and direction, vertical shear and veer – eventually also horizontally and longitudinally [3], [4].

[1] The distribution of Doppler frequency shifts is in principle the same measurand as the time signal of electrical current, but expressed in the frequency domain.

[2] Note that the wavelength of the emitted light varies with the medium – here the air – it is travelling through. The refraction index n_{medium} characterises the medium, e.g. $c_{air} = c/n_{air}$ where $n_{air} \approx 1.0003$ at 20°C and 1atm. Lidars usually use a fixed λ value to convert the Doppler shift in RWS. However, the wavelength in reality varies slightly with temperature, pressure, humidity, etc. Additionally, the potential variability in time of the emitted laser light also affects λ. Hence, calibrating the Doppler shift of the RWS is formally not equivalent to calibrating the RWS. In practice, the aforementioned biases are negligible.

1.3 The need for calibration procedures

1.3.1 Different ways of assessing wind lidar uncertainties

In physics, absolute measurements are derived from fundamental units of length, mass and time. Absolute measurements thus directly relate to the international standard quantities defined in the international system of units (SI). They are opposite to relative measurements, which can be expressed in % of another quantity value[3].

With these definitions, **an absolute measurement system measures absolute quantity values**. The understanding of absolute/relative measurement systems is often the source of confusion and controversial discussions on whether lidars are absolute measurement systems or not. In such discussions, a clear definition of the employed terminology should be provided, as exemplified in this paragraph.

Lidars are measuring instruments, and as such have measurement uncertainties. Their uncertainties can be assessed in different ways, either:

1) by assessing uncertainties of each component of the measurement chain. Such components can for instance be physical parts or numerical processes.
2) by calibrating one of the lidar's measurands (see 1.2). The calibrated measurand is further put through the next steps of the measurement chain to derive uncertainties.

Because of their complex principles (cf. 1.2), the measurement uncertainties of lidars should be carefully assessed. First, at the reconstructed wind parameters level, the assumptions used for reconstruction introduce errors due to e.g. terrain effects, thermal stability, etc. Eliminating such assumptions and measuring a 3D wind-vector is however possible using time-space synchronised systems (cf. the Windscanner system [5]) or bistatic Doppler lidars. Second, at the LOS velocity level, probe volume effects and the chosen method to estimate the Doppler shift create imperfections in lidar measurements. The shape of Doppler spectra in atmospheric conditions are far from ideal Gaussian or Dirac distributions that can be measured under controlled conditions in a laboratory with a hard target or in a wind tunnel. Real-world Doppler spectra from wind lidars can even feature multiple peaks demonstrating how crucial the Doppler shift estimation method is.

1.3.2 Metrological definition of calibration

The fundamental reason for developing calibration procedures is to assign uncertainties to the measurand, i.e. the measured parameter. Calibrated measurands are traceable to international standards since they are related to a reference quantity (itself traceable to the SI).

The International Vocabulary of Metrology, VIM, provides definitions of terms in the field of measurements [6]. In addition, the Guide to the expression of Uncertainty in Measurement, GUM, suggests methodologies for the expression of uncertainties [7]. According to the VIM, a calibration is an:

"operation that, under specified conditions, in a first step, establishes a relation between the quantity values with measurement uncertainties provided by measurement standards and corresponding indications with associated measurement uncertainties and, in a second step, uses this information to establish a relation for obtaining a measurement result from an indication".

[3] E.g. humidity can be measured relatively to the equilibrium vapor pressure of water.

In this definition, “quantity values” refers to the measurements of the reference instrument(s), “indications” refers to the measurand to calibrate. Reformulating, a calibration consists of three parts:

a. Obtaining a relation between the measurand and the reference quantity value;
b. Deriving uncertainties on the measurand by combining uncertainties on the reference together with the measurement process uncertainties;
c. Using the calibration relation in order to establish the correction to apply to the measurement indications (of the instrument being calibrated). This maintains the link in the measurement chain and therefore ensures traceability.

Developing commercial applications of lidars, such as power performance testing or resource assessment, demands calibration procedures providing measurement uncertainties.

Chapter 2

2 Calibration concepts

Considering the levels of measurands in a lidar (cf. 1.2), two different calibration concepts can be identified. The so called “black box” calibration is a direct comparison of the reconstructed output with the corresponding reference quantity. An alternative methodology to the black box consists of calibrating the reconstruction algorithms’ inputs – essentially the LOS velocity and the geometry of the lidar. This method will be further referred to as “white box” calibration.

2.1 The black box methodology

2.1.1 Principles

Using this approach, the lidar is seen as a black box (Figure 2), i.e. a system where the knowledge of the transfer function between inputs and outputs is not relevant or not necessary:

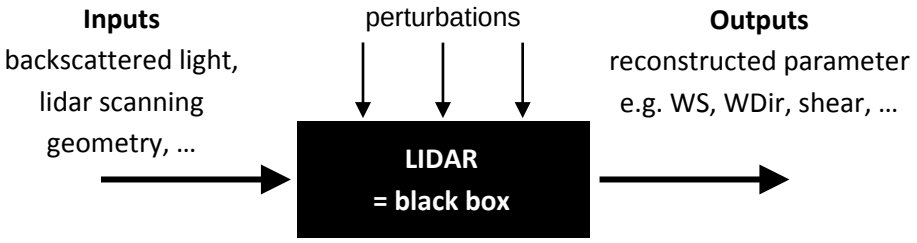

Figure 2. Black box concept of lidar calibration

The black box calibration presents the advantages of: being fast and relatively easy to implement; its results include the uncertainties related to the veracity of the physical model used in the reconstruction algorithm (cf. 2.2.2). However, some disadvantages of the method exist:

- multiple calibrated reference instruments (with certificates) are necessary to calibrate each of the reconstructed parameters. For instance, vertical shear can be measured with anemometers at different heights, veer with multiple wind direction sensors, etc.
- the reconstructed output is a mathematical manifestation. It does not physically exist as it is derived from a number of measurements distant in time and space from each other. Hence, assumptions (e.g. horizontal homogeneity) have to be formulated in the reconstruction algorithms. The assumptions may not be completely justified and strongly related to the characteristics of the calibration site. This will add uncertainty to the reconstructed parameter.
- the calibration procedure and setup is specific to the geometry of the instrument and the output(s) to calibrate.

2.1.2 Black box procedure examples

The wind speed calibration of ground-based lidars is an example of a black box calibration. This calibration is performed by comparing the horizontal wind speeds (HWS) measured by the lidar and reference anemometers placed at different heights on a measurement mast. The configuration of the lidar measurement ranges fits the heights of the reference instruments [8].

For a profiling nacelle lidar, the necessary measurement setup for a black box calibration would require for instance:

a) For horizontal wind speed and wind direction
   - Lidar placed on a stiff platform high enough to allow the beam(s) to not be blocked by the ground in order for the reconstruction algorithm to be available.
     For modern wind turbines, the rotor diameter D_{rotor} is $\sim 100m$. IEC 61400-12 standards require to measure the free wind at an upstream distance of $2.5D_{rotor}$. With a cone or half-opening angle of $\alpha = 15°$, the height of the platform should therefore be greater than $2.5D_{rotor} \cdot \tan(\alpha) \approx 67m$ in addition to a minimum height of 10-20m.
   - A mast with reference instruments (e.g. cup or sonic anemometer, wind vane) mounted at the same height as the reference height of the lidar's reconstructed parameter. This height is usually the optical centreline.
   - Accurate detection of the lidar beam or centreline. This may be extremely difficult to achieve, particularly if no beam is present at the centre of the scanning pattern.

b) For vertical wind shear and veer, reference wind speed and direction instruments measuring at several heights ranging between the minimum and maximum measurement heights of the lidar, e.g. from 10m to 150m.

2.2 The white box, a generic method to calibrate a wind lidar

2.2.1 Principles

The reconstruction algorithms combine radial wind speed measurements, beam localisation quantities – e.g. inclination and roll angles of the beam – and the geometry of the scanning pattern. The white box calibration requires having access to the reconstruction algorithms and being able to:

- calibrate the lidars' internal inclinometers, both for the tilting and rolling;
- verify the scanning pattern geometry, e.g. opening angle between two beams, or cone angle for a circular scanning pattern;
- calibrate the RWS, measured by the lidar along some or all of the beams.

2.2.2 Advantages of the white box methodology

The main advantages of the white box are a calibration of a physically existing quantity and a lower sensitivity to assumptions (e.g. flow homogeneity). The uncertainty estimation of any reconstructed parameter is theoretically permitted by the white box approach.

On the negative side, the calibration duration is longer for multi-beam lidars as each successive LOS needs to be calibrated. Alternatively, one or two RWS calibrations combined with a model of deviations between

beams could be used. To implement calibration procedures for commercial lidars, the reconstruction algorithms will have to be provided (as a minimum, at least to the calibration laboratory). The physical veracity of the reconstructed parameter has to be addressed. In other words, the underlying physics behind the reconstruction algorithm must be correct and therefore verified once for each parameter and type of lidar.

Additionally, one can discuss whether the uncertainties on reconstructed parameters using the white box calibration are the same as those obtained with the black box. It should not be expected that uncertainties using the white or the black methodologies are exactly the same since the black box includes the uncertainties related to the veracity of the physical model used for the reconstruction. They should however show similar order of magnitudes.

2.2.3 A generic nacelle lidar calibration method

According to dictionaries, *generic* means applicable or referring to all members of a group. The antonym of *generic* is specific.

The white box calibration can be applied to all profiling nacelle lidars, and possibly to any lidar irrespective of its application. Thus, the method is generic. Indeed, all Doppler lidars measure the RWS, the calibration of which is central in the white box approach. The data requirements and measurement setup – described in 3.1 and 3.5 respectively – are expected to be similar for any lidar.

In contrast, different lidars would provide specific reconstructed parameters, requiring measurement setups specific to potentially each reconstructed parameter and to the geometry of the lidar (cf. 2.1.2).

Note: in the next sections of this report only the white box methodology is considered. The method is illustrated with the calibrations of the ZephIR Dual Mode lidar and an Avent 5-beam Demonstrator lidar carried out at DTU's test site for large wind turbines, Høvsøre, between November 2014 and April 2015.

2.2.4 Main steps of the white box calibration

The main steps of the white box calibration are:

a. **Geometry verification**: the parameters characterising the geometry of the scanning pattern must be measured in order to check the manufacturer's specifications, e.g. cone or half-opening angle(s). Knowing the geometry is necessary for reconstructing wind parameters (e.g. horizontal wind speed and direction). These values are also used for instance to correctly configure the measurement range of the lidar during the calibration.

b. **Sensing range verification**: nacelle lidars are measuring in a flow that has a longitudinal gradient. Therefore the sensed wind speed will depend critically on where the wind is sensed. For this reason, the sensing range should be verified.

c. **Inclinometers calibration**: to correct for the indications of the inclination angle φ involved in the vertical projection of the reference HWS, and assign uncertainties to φ.

d. **RWS field measurements**: measurement data collection, with the lidar beam carefully positioned close to a reference instrument (see 3.2).

e. **RWS uncertainty assessment**: combining uncertainties from the reference and measurement process.

f. **Reconstruction of wind parameters**: by combining LOS velocities.

g. **Reconstructed parameters uncertainty assessment**: for instance using the GUM, or any other relevant uncertainty derivation method (e.g. Monte-Carlo or Bootstrap).

Since the geometry and the inclination angle are used respectively for the range configuration and the data analysis of the RWS measurement, steps a and c (see detailed procedures in [9] and [10]) should preferably be performed prior to d. Steps d and e correspond to the RWS calibration. Steps f and g are specific to each reconstructed parameter and each type of lidar and will not be detailed in this report.

Note: steps d and e are generic, while steps a, b, c, f, g are specific to one type of lidar. Examples of wind parameter reconstruction and uncertainty assesment illustrating how to combine the LOS velocities uncertainty components are also given in [9] and [10].

Chapter 3

3 RWS calibration procedure

This section details the steps of the white box methodology corresponding to the calibration of the RWS (see 2.2.4, step d). In addition, the calibration of the lidar's inclinometers is the object of a paragraph since its results are used in the data analysis.

3.1 Data requirements

A lidar senses the wind contained in a probe volume located along the beam. Thus, the chosen reference quantity value $Ref_{eq\ RWS}$ is the dot product of the LOS unit directional vector and the wind velocity field at the point of focus for a CW lidar and centre of the range gate for a pulsed one, i.e. the projection of the horizontal wind speed (HWS) onto the LOS direction:

$$Ref_{eq\ RWS} = \langle HWS \rangle_{vec} \cdot \cos\left(\langle \varphi_{physical} \rangle\right) \cdot \cos(\langle \theta \rangle_{vec} - LOS_{dir}) \qquad \text{(eq. 2)}$$

Where: $\langle\ \ \rangle$ and $\langle\ \ \rangle_{vec}$ denote respectively scalar and vector averages over the chosen time period, HWS the horizontal wind speed, $\varphi_{physical}$ the physical inclination angle between a horizontal plane and the LOS, θ is the wind direction, and LOS_{dir} is the bearing or LOS direction. θ and LOS_{dir} must be defined in the same reference frame, e.g. clockwise and $0°$ for North.

Theoretically, the correct reference quantity value is the average of the instantaneous projection. If $\varphi_{physical}$ is constant, it can be demonstrated that using the vector averages $\langle HWS \rangle_{vec}$ and $\langle \theta \rangle_{vec}$ provides the same values when projecting in the horizontal plane. Since the lidar is in a stiff position, on the ground, the standard deviation of the inclination is: $stdv\left(\varphi_{physical}\right) \ll \langle \varphi_{physical} \rangle$. Thus, the approximation made implicitely in (eq. 2) can be accepted.

The derivation of the reference quantity value $Ref_{eq\ RWS}$ (eq. 2) also implicitely neglects the contribution of the vertical component w of the wind vector to the RWS. This contribution can be expressed as:

$$\langle w \rangle \cdot \sin\left(\langle \varphi_{physical} \rangle\right) \qquad \text{(eq. 3)}$$

As an example, for $w = 0.1\ m/s$ and the inclination $\varphi_{physical} = 1.6°$ in the setup 4.2, we obtain $\langle w \rangle \cdot \sin\left(\langle \varphi_{physical} \rangle\right) \approx 0.1 \cdot \sin(1.6°) \approx 0.003\ m/s \ll Ref_{eq\ RWS}$. If a sonic anemometer is used as a reference instrument, the impact of this contribution can be further limited by filtering the inflow angles (e.g. between -2° and +2°) or by simply adding the projection of the vertical component to $Ref_{eq\ RWS}$ (eq. 2).

The RWS calibration is applied to time-averaged data. The minimum duration of the averaging period depends on the measurement frequency. For power performance measurements, the standard duration is 10 minutes[4]. To ensure comparable time-averaged measurements between the reference instrument and the lidar, the averaging period must contain a minimum number of data points (e.g. three 10-min periods).

In the RWS calibration procedure, the required data are:

- **For the reference instrument(s):** vector means of the wind direction (θ) and horizontal speed [11]. Note that vector and scalar averages of HWS are defined as:

$$\begin{cases} \langle HWS \rangle_{vec} = \sqrt{\langle u \rangle^2 + \langle v \rangle^2} \\ \langle HWS \rangle_{scalar} = \langle \sqrt{u^2 + v^2} \rangle \end{cases} \quad \text{(eq. 4)}$$

  where u and v are the two components of the HWS vector.
- **For the lidar**: the RWS and tilt angle.

Notes:

- In (eq. 2), the LOS direction is estimated via measurement data analysis (cf. 3.6.1).
- The lidar measurements and the reference instrument(s) must be synchronised in time. A synchronisation tolerance of $\pm 1\%$, i.e. ± 6 seconds for 10-min averaging periods, is acceptable according to the latest revision of IEC-12-1 (see [12]).

3.2 Beam positioning techniques

As the radiation wavelengths of lidars are usually not in the visible spectrum ($\sim 1.55\ \mu m$), accurately positioning and detecting the beam is possible either by performing a hard target test or visualising the laser beam with an infrared sensitive card or an infrared camera.

A hard target test consists of detecting the beam by blocking it with a reflective surface, and then measuring its position. When the beam is blocked, the response of the lidar measurements shows extreme levels of carrier-to-noise ratios (CNR) compare to those observed in normal atmospheric conditions. Here, the difference between pulsed and CW lidars lies in the necessity for a CW lidar to hit a moving target. The beam position of a pulsed lidar can for instance be detected using shutters (see Figure 3).

Examples of responses for pulsed and CW lidars are displayed in Figure 3 and Figure 4 respectively. In Figure 3, LOS4 hits the hard target at approximately 255m while the other LOS show normal levels. In Figure 4, the left picture shows the response of the CW lidar when the beam hits a moving target, e.g. a cup anemometer, at the bottom of the circular scanning pattern; the right picture corresponds to the same situation with the moving target stopped.

[4] The 10-minute duration is conveniently used in the industry and power performance standards. Originally, it corresponded to the spectral gap reported historically by Van der Hoeven in 1957. However, independent and more recent studies questioned the existence of such a spectral gap in the atmospheric boundary layer. Thus, power curves based on other durations may also be studied, e.g. 5-min or 2-min averages. In such a case, the lidar should be calibrated using the same averaging duration.

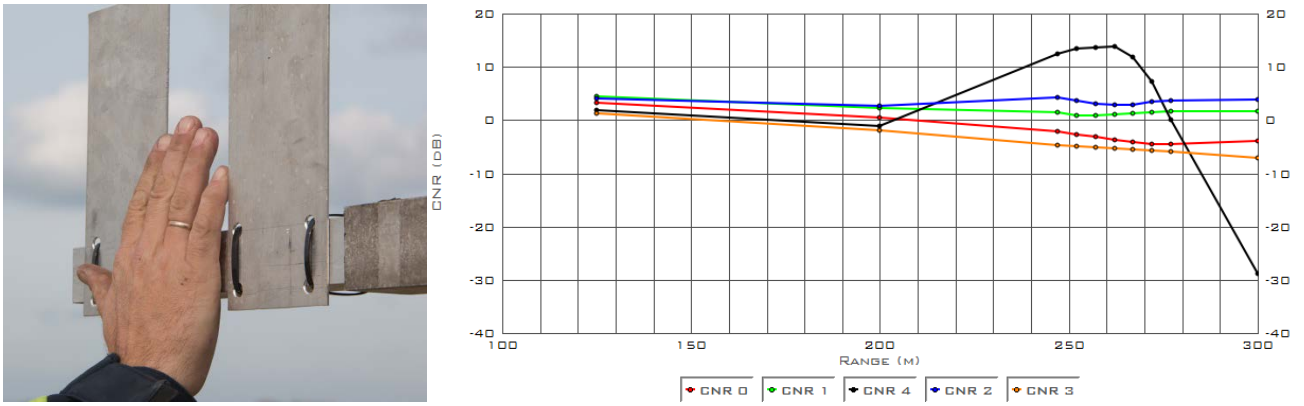

Figure 3. Shutters (left) and CNR response (right) of a pulsed lidar hitting a hard target: example of the 5-beam Demonstrator (Avent).

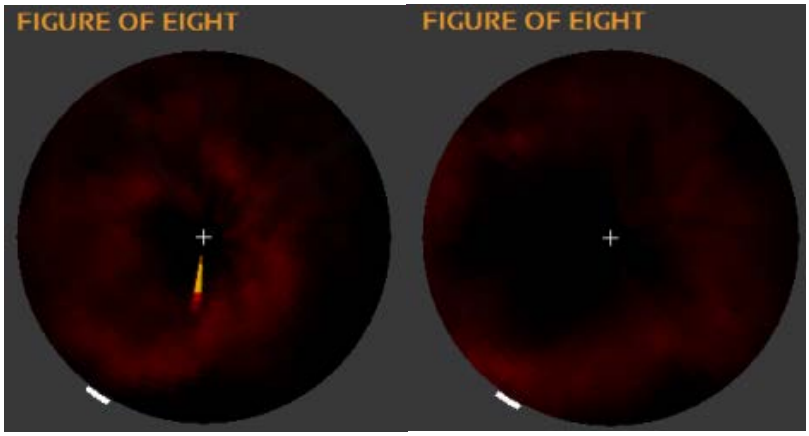

Figure 4. Response of a CW lidar hitting a moving hard target: example of the ZDM lidar using the 'figure of eight plot' (polar plot of LOS velocity, the backscatter strength is reflected in the colour levels)

3.3 Inclinometers calibration

A calibration procedure for two-beam nacelle lidars inclinometers has been demonstrated in [13]. The procedure consists in: finding the beam position, measuring the distance and height using e.g. a theodolite, deriving the tilt and roll angles and compare them to the lidar indicated values. The procedure provides simultaneously the inclinometers calibration and the opening angle value between two beams. It has been applied repeatedly, and has demonstrated its ability to provide consistent calibration results (tilt and roll).

The procedure can be adapted to multi-beam lidars by:

- defining a $0°$ tilt angle, e.g. when the optical centre line of the lidar is horizontal;
- considering opening angles between each pair of beams, α.

The procedure can also be adapted to scanning lidars by detecting the beam at different positions of the scanning pattern.

The inclinometers calibration results are further considered through the linear regressions' gains a_{tilt}, a_{roll} and offsets b_{tilt}, b_{roll}.

3.4 Inclination angle correction

The physical inclination of the beam $\varphi_{physical}$ is derived by correcting the lidar indication $\varphi_{indicated}$:

$$\varphi_{physical} = a_{tilt} \cdot \varphi_{indicated} + b_{tilt}$$

The 10-min average value of $\varphi_{physical}$ is used in the projection (eq. 2). With the measurement setup described in 3.5, $\varphi_{physical} \approx 1.6°$. The elevation angle can instead be measured using e.g. a theodolite, and then used as a constant value instead of the lidars' measurements.

Note: the roll angle is not used in the projection of the reference HWS (eq. 2). However, the lidar indicated roll is corrected in the same manner and the resulting value can be used for filtering. This filter ensures that the beam height stays within a narrow range centered on the reference instrument.

3.5 RWS measurement setup

A typical measurement setup for the RWS data collection is described in [13]. The lidar beam points towards a reference instrument that provides both wind speed and direction (see Figure 5).

Formally, the calibration setup must replicate as closely as possible the measurement conditions in which the lidar will be measuring. For nacelle lidars, this implies a next-to-horizontal LOS. And, since in power performance standards the free wind must be measured (~2.5D upstream of the rotor plane), the measurement range must be of the same order, i.e. 200m-300m.

Figure 5. Calibration measurement setup of ZDM (ZephIR) and the 5-beam Demonstrator (Avent) at DTU Wind Energy test site, Høvsøre (DK)

Depending on the height of the reference instrument, maintaining a close-to-horizontal LOS may demand installing the lidar at similar height, e.g. on a platform. With a relatively small mast, the lidar can be positioned on the ground and its beam tilted up (see Figure 5). The elevation angle should however be limited to avoid measurement errors due to the inhomogeneity within the inclined probe volume and caused by vertical shear and veer as well as an eventual sensing range error. In other words, with an inclined beam, the probe volume senses winds over a range of heights. The vertical shear profile may therefore introduce an error in the RWS measurement. The maximum value of the beam elevation depends both on the height of the reference instrument and the physical tilting of the beam (equivalent to height and horizontal distance). A model of the effect of the vertical shear within the probe volume is given in Annex A.

Usually, the measurement range is defined along the lidar's optical centreline. If α is the opening angle between the centreline and the LOS to calibrate, the adequate range D_{config} is:

$$D_{config} = D_{physical} \cdot \cos(\alpha) \quad \text{(eq. 5)}$$

Where $D_{physical}$ is the physical distance between the lidar and the reference instrument. Formally, the origin of the laser beam should be used to measure $D_{physical}$. If such a point exists, the origin is either the intersection of the LOS or the apex of the cone angle, respectively for multi-beam and circularly scanning lidars. Given that the origin can be defined or estimated, $D_{physical}$ can be accurately measured, for example by using a range-finding theodolite ('total station') or high-resolution GPS.

If a single instrument is used as reference (e.g. a sonic anemometer providing both the reference wind speed and wind direction), the beam must be located close enough, and more importantly at the same height, to ensure maximum correlation and minimise biases due to both vertical and horizontal shears. However, potential wake effects for intrusive instruments should also be taken into account. Typically, a horizontal separation of $\sim 1 - 2m$ can be used. If two instruments (e.g. a cup anemometer providing the wind speed and a wind vane providing the reference wind direction) installed side by side at the same height are used, the beam should be located close to the one measuring the wind speed since it is the main factor driving $Ref_{eq\ RWS}$. In our example, we have used a cup anemometer as wind speed reference and a sonic anemometer as wind direction reference. They were mounted on two masts separated by $\sim 5m$ so they could be mounted at the same height a.g.l., as shown in Figure 6.

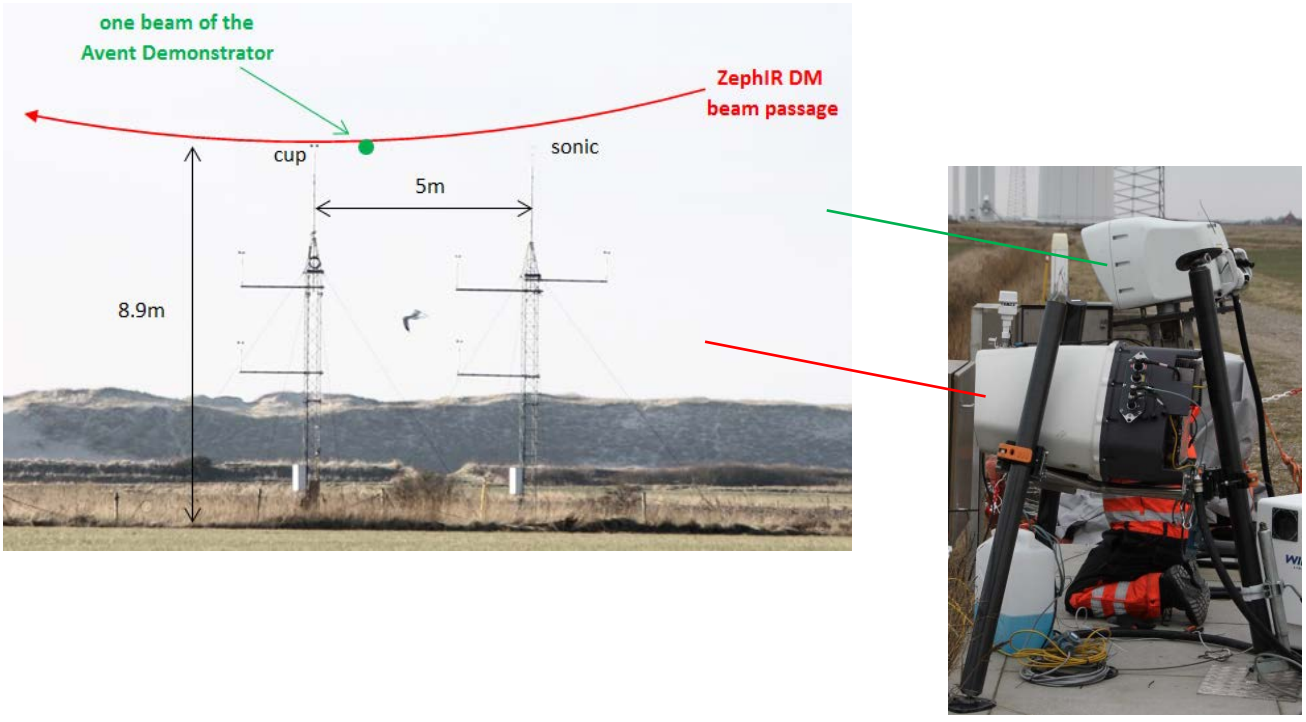

Figure 6. Schematic of the 5-beam Demonstrator (in green) and ZDM (in red) beam positions, DTU Wind Energy test site, Høvsøre (DK)

Evidence of the detection of the beam position close to the reference instruments must be reported in the calibration report.

3.6 Data analysis and calibration results

This section corresponds to the analysis of the data collected during the RWS calibration (cf. c in 2.2.4). It is thus considered that, prior to this step, the geometry verification and inclinometers calibration have been performed, e.g. using the method in [13]. The data analysis aims at establishing a relation between the lidars indicated RWS and the reference equivalent value (cf. 3.1):

$$Ref_{eq\ RWS} = \langle HWS \rangle_{vec} \cdot \cos\left(\langle \varphi_{physical} \rangle\right) \cdot \cos(\langle \theta \rangle_{vec} - LOS_{dir}) \quad \text{(eq. 2)}$$

At this stage, the LOS direction is the last unknown (other quantities measured and calibrated) which therefore needs to be evaluated.

3.6.1 LOS direction evaluation

The LOS direction evaluation is a 2-step process. First, the lidar response to the wind direction is fitted to a function (cf. 3.6.1.1) in order to retrieve an approximate LOS direction in the frame of the reference wind direction sensor. Then, a process based on residual sum of squares (RSS or SSR) is applied, yielding the accurate and final value of the LOS direction [13].

3.6.1.1 Wind direction response fitting – approximate LOS_{dir}

The LOS direction is first evaluated by plotting normalised RWS as a function of the measured wind direction (θ). In this analysis, all wind directions sectors are valid except for site related specifications (e.g. tower shadowing, presence of obstacles, wakes from neighbouring turbines, etc).

The normalised RWS is $\langle RWS_{norm} \rangle = \langle RWS \rangle / \left(\langle HWS \rangle_{vect} \cdot \cos\langle \varphi_{physical} \rangle \right)$. As a lidar measures the component of the wind vector projected onto the LOS, the fitting function f_{fit} is for example:

- A cosine for a pulsed lidar: $f_{fit}(\theta) = gain \cdot \cos(\theta - \theta_0) + offset$
- A rectified cosine for a homodyne CW lidar: $f_{fit}(\theta) = gain \cdot |\cos(\theta - \theta_0)| + offset$

The fitting process yields gain and offset values ideally close to 1 and 0 respectively, while θ_0 provides an approximation of the LOS direction: $LOS_{dir} \approx \theta_0$.

Homodyne CW lidars measure only the magnitude of the Doppler shift – not its sign – which translates into positive LOS velocities. In such a case, a rectified cosine must be used. The ambiguity in the fitting, i.e. the two different solutions for θ_0, is resolved by choosing the value corresponding to the expected bearing of the beam, e.g. using satellite imaging or GPS data.

3.6.1.2 Residual sum of squares – accurate LOS_{dir}

The residual sum of squares (RSS) process is further used to refine the estimation of the LOS direction. The steps of the process are:

- Restrict the valid dataset to a wind direction sector based on the estimated θ_0, e.g. $\pm 40°$
- Definition of a projection angle θ_{proj} range, e.g. $\theta_{proj} = \theta_0 \pm 1°$
- Choosing a step within that range: e.g. $0.1°$
- For each projection angle θ_{proj}, a linear regression is performed between the period-averaged RWS $\langle RWS \rangle$ and the equivalent quantity value: $\langle HWS \rangle_{vec} \cdot \cos\big(\langle \varphi_{physical} \rangle\big) \cdot \cos(\langle \theta \rangle_{vec} - \theta_{proj})$
- The RSS of each linear regression is reported and plotted vs. θ_{proj}
- A 2nd order polynomial is fitted to the curve.
- Finally, the LOS direction is the minimum of the parabola (see Figure 7).

The last step assumes that a minimum of the residuals ($\sum RWS - HWS_{proj}$) is obtained when the HWS is projected on the correct LOS direction.

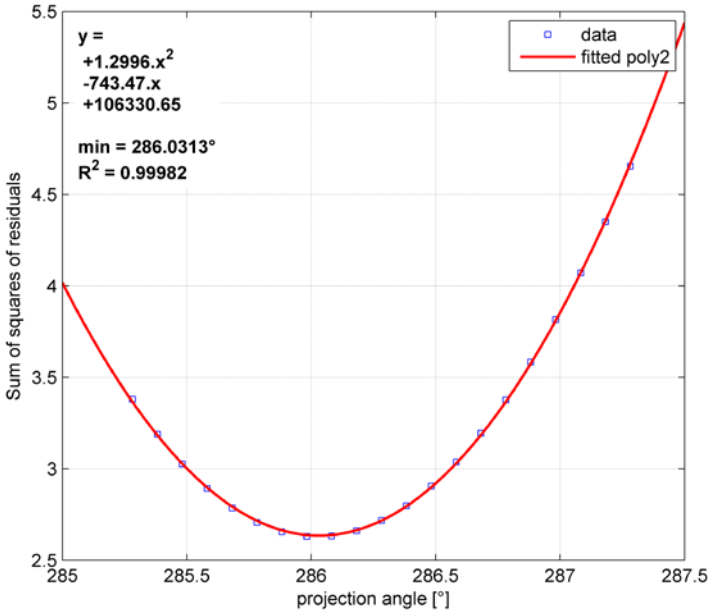

Figure 7. LOS direction evaluation using the RSS process

3.6.2 Calibration results: linear regressions on raw and binned data

The reference equivalent RWS (eq. 2), can now be derived and compared to the lidar indicated RWS. Forced and unforced linear regressions are performed on:

- the raw data: i.e. the period-averaged (10-minute) measurements of RWS and $Ref_{eq\ RWS}$
- the binned data: bin-averaged measurements are obtained using 0.5 m/s RWS bins and a minimum number of 3 points per bin.

Note on binning method: the minimum valid RWS is equal to the minimum valid HWS ($4\ m/s$) multiplied by the minimum projection ($\cos(40°) \cdot \cos(1.6°)$). Thus the minimum bin corresponds to:

$$RWS \in [2.75\,;3.25]\ m/s$$

Similarly, the maximum bin is:

$$RWS \in [15.75\,;16.25]\ m/s$$

Figure 8 presents an example of both raw and binned calibration results. The forced and unforced linear regressions' equations are respectively displayed in black and red. The intercept in the unforced regression is expected to be close to 0. In practice, using the forced regression is also more convenient to compare calibration results[5]. Thus, the forced regression equation will be preferred. Moreover, binned data should be used in order to avoid risking the calibration results to be influenced by data points lying in the same range of atmospheric conditions (e.g. too many points at low wind speed vs. lack of points at higher wind speed).

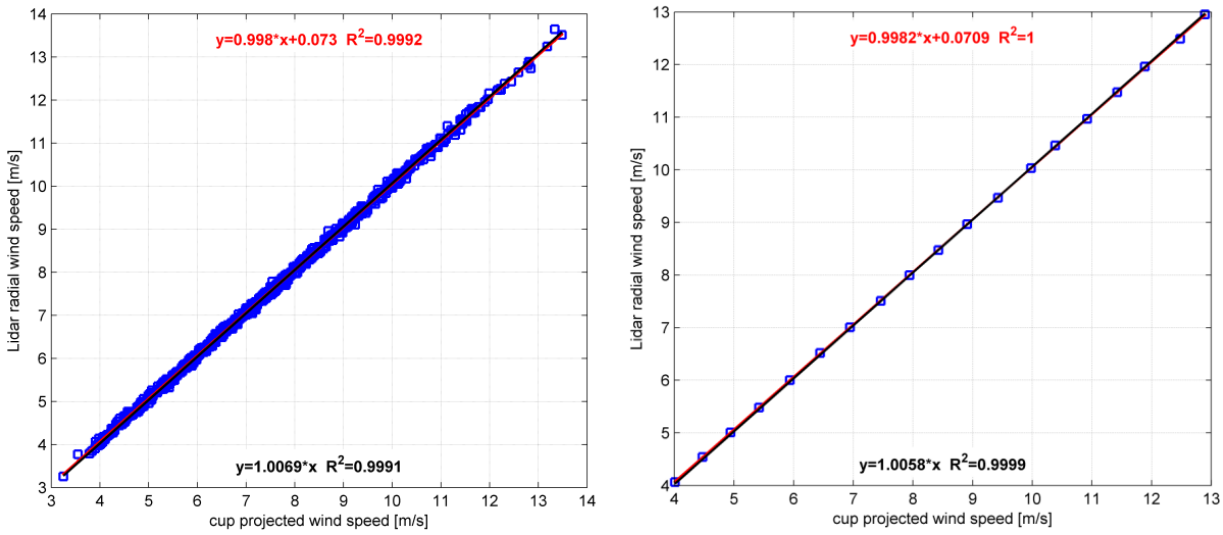

Figure 8. RWS calibration results example: raw (left) and binned (right) data

[5] Additionally, whether the unforced or the forced regression is used to correct the RWS, the result is not affected significantly. For example, if $RWS_{indicated} = 10\ m/s$, using the results in Figure 8, we obtain respectively $RWS_{corrected} = 9.947\ m/s$ (unforced) and $RWS_{corrected} = 9.942\ m/s$ (forced). See option 2a in 5.4.2 and option 3a in 5.4.3.

Chapter 4

4 RWS calibration of profiling nacelle lidars: examples

4.1 Geometry and basic information on the Avent 5-beam Demonstrator and ZephIR Dual Mode (ZDM) lidars

In this section, the basic measurement principles and geometry of two commercially developed profiling nacelle lidars are presented.

4.1.1 The 5-beam Avent Demonstrator lidar

The 5-beam Demonstrator lidar (Figure 1) is a heterodyne pulsed Doppler system developed by *Avent Lidar Technology* for research and development purposes. It measures successively the wind along five LOS, with a measurement frequency of $1\,Hz$ (i.e. 1 second / LOS). At each LOS measurement, up to 10 ranges are measured simultaneously (Figure 9).

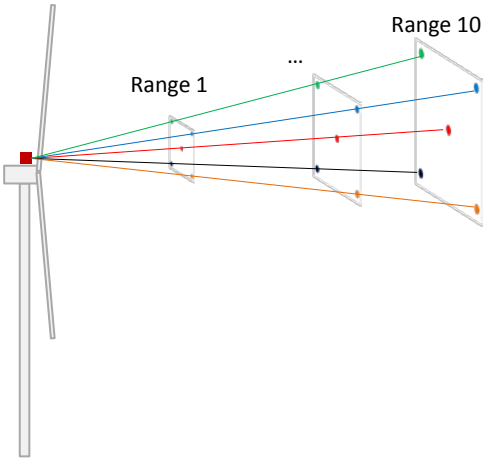

Figure 9. Schematic of the 5-beam Demonstrator lidar (Avent) mounted on the nacelle of a wind turbine

Two configurations are available: cross or square (see Figure 10). The pattern is pre-configured as it requires adjusting the position of internal parts (e.g. telescopes). In the UniTTe project, the square pattern has been chosen: when mounted on the nacelle, if there is no yaw misalignment, $RWS0 \approx HWS$; two beams are located at the lower and upper heights, allowing wind speed and direction reconstruction similarly to two-beam nacelle lidars.

The half-opening angle – i.e. the angle between LOS0 and another LOS – is $\alpha = 15°$ (manufacturer specification). At the lower and upper heights, the corresponding half-opening angle between e.g. LOS1 and LOS2 is $\beta = \mathrm{atan}\left(\tan\alpha/\sqrt{2}\right) \approx 10.73°$.

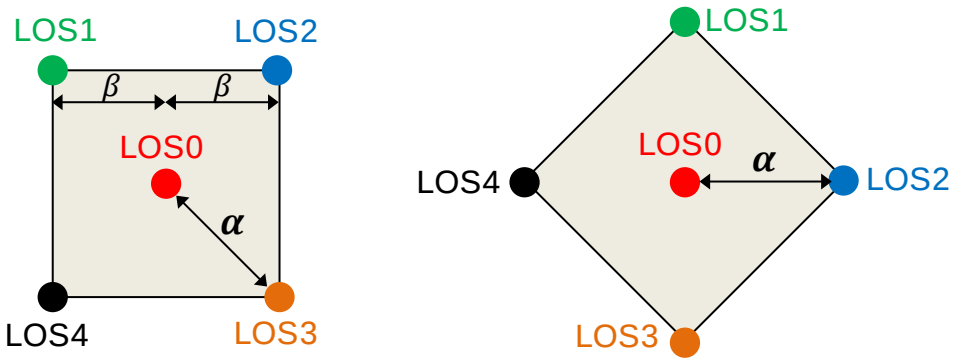

Figure 10. 5-beam Demonstrator lidar LOS geometry: square (left) and cross (right) configurations

Finally, as the 5-beam Demonstrator is a pulsed system, its probe length depends mainly on the pulse duration and is constant with the measurement range. Its probe length is $\sim 25m$, thus the minimum range is $\sim 50m$. Depending on atmospheric conditions (aerosols), the maximum range is approximately 300-350m.

The five LOS use the same laser source and optical chain, except for the telescopes. Thus, each LOS should be calibrated. This is what has been performed in Høvsøre, one LOS after another. As the calibration of one LOS takes usually 3-6 weeks, the process is long and an alternative solution has been proposed in 2.2.2.

4.1.2 ZephIR Dual-Mode lidar

The ZDM lidar (Figure 1) is a homodyne continuous wave Doppler system developed by *ZephIR Lidar*. It is an upgrade of the ground-based Z300 lidar allowing to place it horizontally on the nacelle of a turbine. ZDM uses the rotation of a prism to measure in a fixed conical scanning pattern (Figure 11). The cone angle is thus constant: $\alpha = 14.97°$ (manufacturer specification).

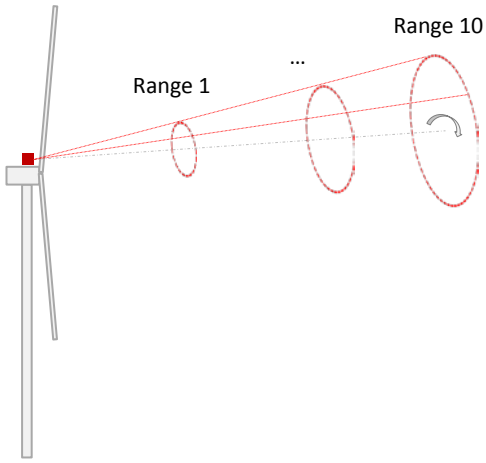

Figure 11. Schematic of the ZDM lidar (ZephIR) mounted on the nacelle of a wind turbine

At one specific range, the scanning pattern is circular. Each revolution takes one second and, on average, 48.8 azimuth sectors are measured (see Figure 12). One LOS velocity is obtained by averaging Doppler spectra over an azimuth sector of $360°/48.8 \approx 7.38°$.

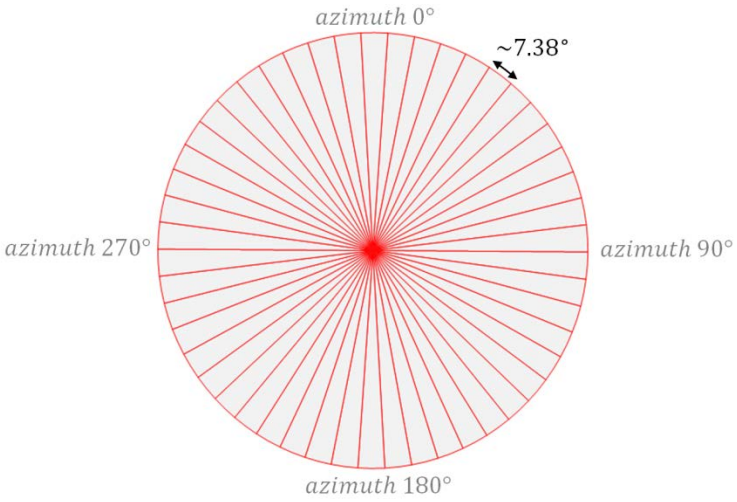

Figure 12. Scanning geometry of the ZDM lidar: ~50 LOS / revolution

User-selected ranges are measured successively by re-focusing the laser beam. ZDM is able to measure at ranges between $10 - 300m$, and a maximum of 10 ranges can be configured. However, being a CW lidar, the probe length increases with the range ($\propto Range^2$) from $\sim 10cm$ at $10m$ to $\sim 60m$ at the range of $300m$.

The ZDM lidar features a single "scanning" beam. The optical chain from the laser source to the telescope is the same independently of the azimuth position – only the position of the prism differs. Therefore, the calibration of the LOS velocity is performed by computing averages of LOS velocities contained in a single azimuth sector (see Figure 13). However, the chosen azimuth sector should sweep points at the same height. This can be achieved with minimum bias at long range and by taking the "top" or "bottom" sectors (e.g. for azimuth angles $\in [179°; 181°]$).

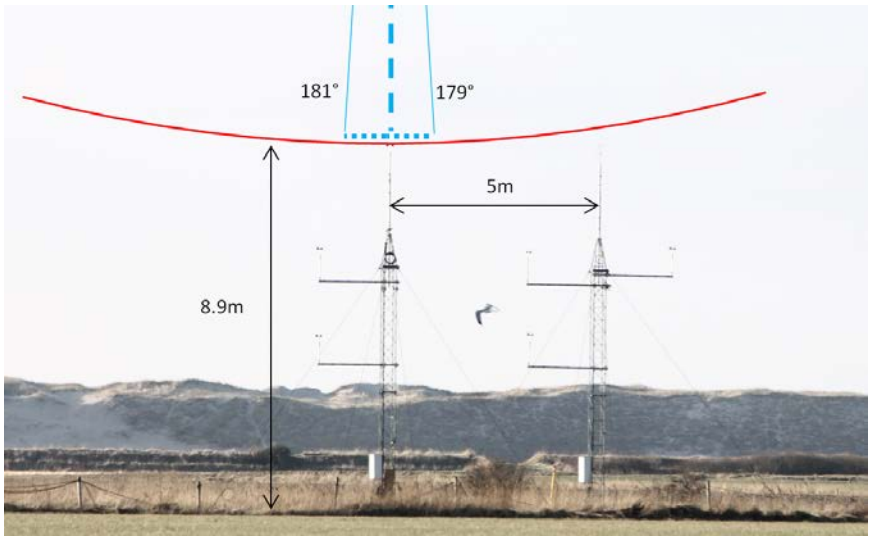

Figure 13. Averaging LOS velocity measurements in a narrow azimuth sector (ZDM lidar)

4.2 Measurement setup

Both the 5-beam Demonstrator and ZDM lidars have been calibrated at DTU Wind Energy's test site, Høvsøre, DK. The measurement setup providing the required data (3.1) of the RWS calibration campaign is:

- Reference instruments (Figure 6):
  - one cup anemometer and one sonic anemometer providing wind speed and direction measurements respectively
  - top-mounted on two met. masts distant by ~5m
  - height a.g.l.: $H_{mast} = 8.9m$
- Lidars placed on solid ground (Figure 5)
  - ~262m away from the reference instruments
  - slightly tilted up for the beam to be located close to the reference instruments:

$$\varphi_{physical} = \text{atan}\left(\frac{H_{mast} - H_{lidar}}{D_{physical}}\right) \approx 1.6°$$

4.3 Inclinometers calibration results and geometry verification

The inclinometers calibration was performed prior to the installation of the lidars for the RWS calibration campaign. We used hard target methods and a theodolite to measure the coordinates of the position of the beam. The procedure is specific to each lidar and will be detailed in separate calibration reports.

Figure 14 shows the results of the tilt inclinometer calibration. With $\varphi_{indicated}$ being the tilt angle indication from the lidar and φ_{BE} the best estimate of the tilting, the calibration relation is:

- For the 5-beam Demonstrator lidar: $\varphi_{BE} = 1.0123 \cdot \varphi_{indicated} + 0.0471$
- For ZDM: $\varphi_{BE} = 0.9950 \cdot \varphi_{indicated} + 0.2382$

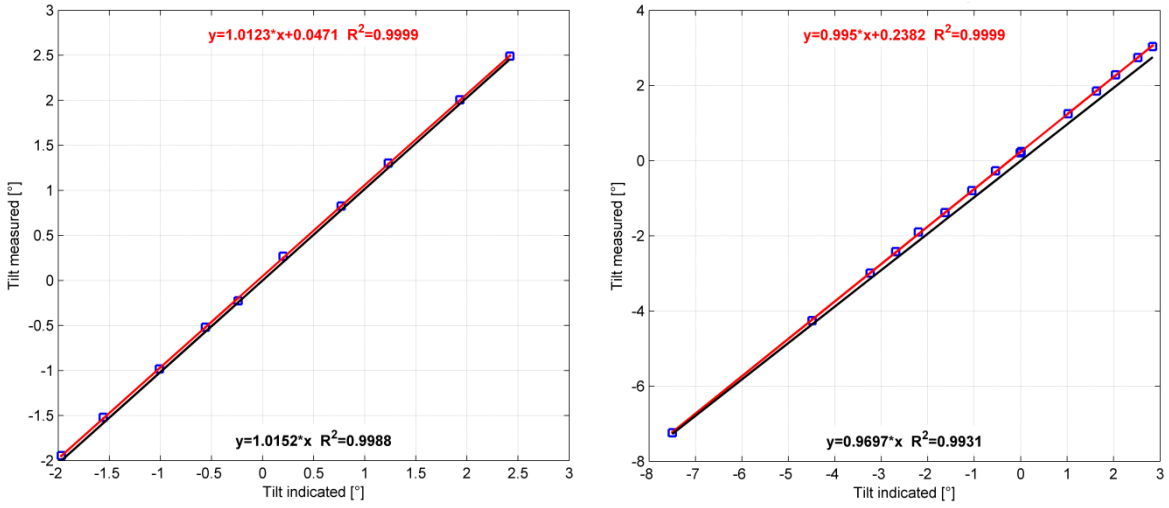

Figure 14. Calibration of the tilt inclinometer: 5-beam Demonstrator (left) and ZDM (right) lidars

The geometry verification is performed simultaneously as the inclinometers calibration. The measured geometry is:

- **For the 5-beam Demonstrator**, the half-opening angles between the central LOS and the others:

$\alpha_{LOS0-LOS1}$	$\alpha_{LOS0-LOS2}$	$\alpha_{LOS0-LOS3}$	$\alpha_{LOS0-LOS4}$
$\mathbf{15.07°}$	$15.09°$	$15.11°$	$15.06°$

  The measurements have been performed at ~30m. Because of the design of the 5-beam Demonstrator (internal positions of the telescopes), the half-opening angles are theoretically slightly larger than $15°$ at this range, which is consistent with the verification results.
- **For ZDM**, the cone half-angle $\alpha_{measured} = 15.05°$ and agrees well with the manufacturer specified and theoretical value of 14.97°.

The geometry verification[6] results are consistent with the manufacturer's specifications ($< 0.5\%$ deviation). Consequently, the manufacturer's specified geometry values may be used for reconstruction of wind parameters.

4.4 LOS direction evaluation

4.4.1 1st estimation: approximate LOS direction

The responses of the normalised RWS measurements to the wind direction and corresponding fitting results of the 5-beam Demonstrator and ZDM lidars are illustrated in Figure 15. The gains and offsets of the fitted functions are both close to the expected values of 1 and 0. The fitting methods described in 3.6.1.1 are therefore validated for both lidars.

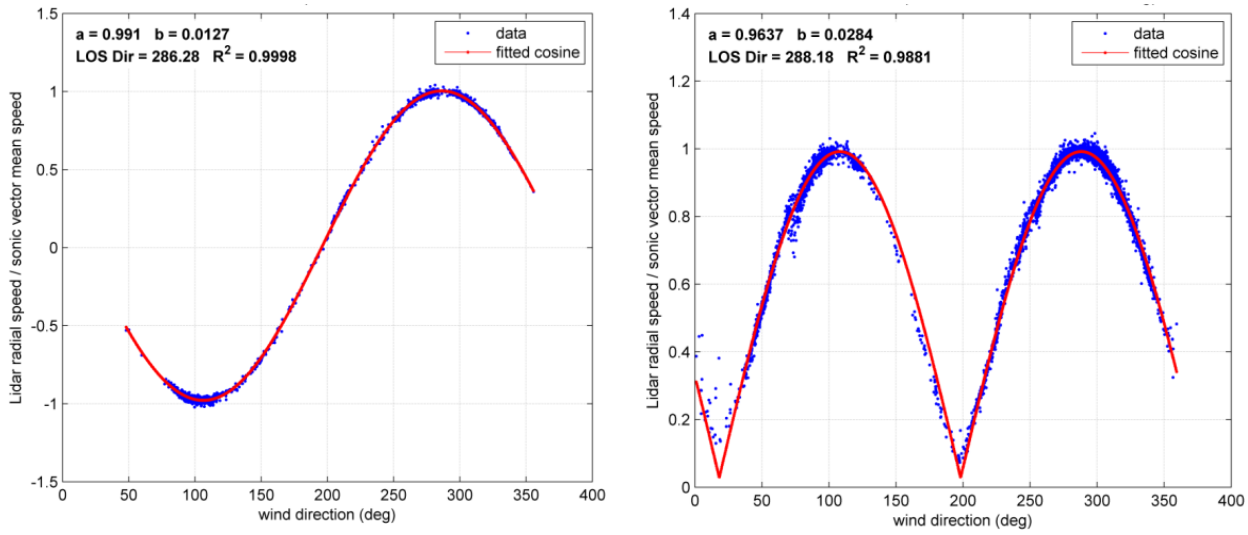

Figure 15. Cosine and rectified cosine responses of the 5-beam (left, LOS0) and ZDM (right) lidars

[6] The assessment of measurement uncertainties would be required in order for the verification to formally be a calibration.

4.4.2 2nd estimation: accurate LOS direction

The RSS process (3.6.1.2) results are displayed in Figure 16. They show a difference of $\sim 0.3 - 0.7°$ between the LOS direction and its first estimation θ_0. Two plausible explanations affecting the first estimation are: lower-quality RWS measurements for wind directions orthogonal to the LOS; asymmetry of the wind direction sensor geometry, here a Gill sonic R3-100 anemometer.

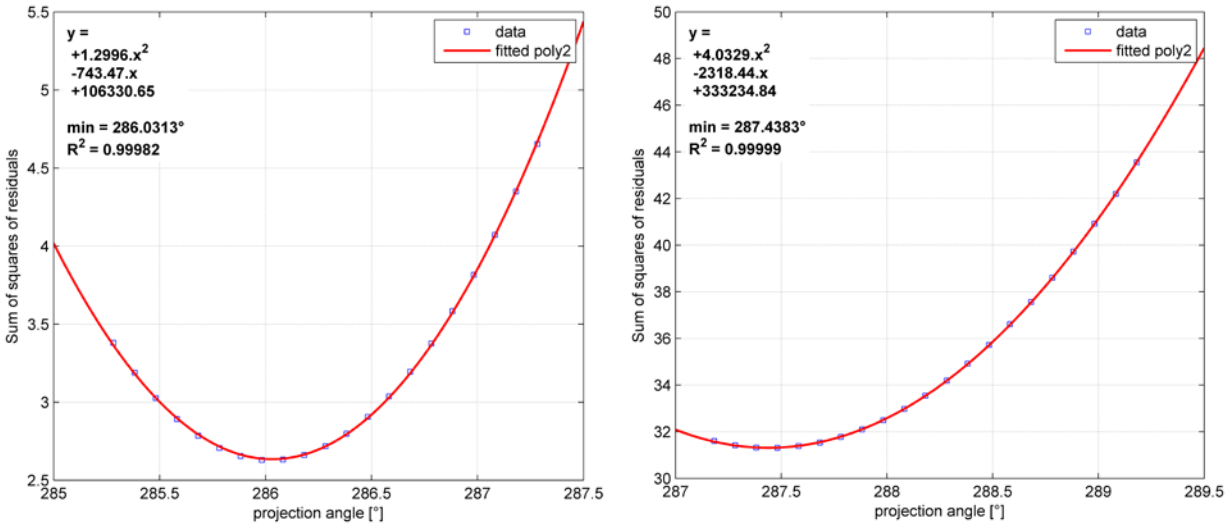

Figure 16. LOS direction evaluation using the RSS process: 5-beam (left, LOS0) and ZDM (right) lidars

The LOS direction is found to be $286.03°$ for the example of LOS0 in the 5-beam Demonstrator lidar, and $287.44°$ for the ZDM lidar (bottom sector).

These values are expressed in the frame of the sonic anemometer used for the wind direction measurement. The sonic anemometer is aligned to the absolute North, with a mounting uncertainty roughly estimated to $1 - 2°$. Using GPS coordinates, the LOS directions for the 5-beam and ZDM lidars are estimated respectively to $285.4°$ and $285.8°$. Thus, the results of the LOS direction evaluation are consistent with these values.

4.5 RWS calibration results

Figure 17 corresponds to the RWS calibration results of:

- for the 5-beam Demonstrator, LOS0
- for ZDM, the LOS velocity is averaged over the $[179° ; 181°]$ azimuth sector.

Both raw and binned results are plotted and demonstrate the low scatter that can be observed in the RWS calibration methodology. The 10-min average RWS data are however filtered in order to remove outliers from the analysis. Among others, the main filters providing the valid dataset are:

- Cup anemometer HWS $\in [4; 16]$ m/s: uses the HWS range for which the cup anemometer is calibrated.
- Sonic anemometer wind direction $\in LOS_{dir} \pm 40°$: removes outliers due to wind direction measurement errors, itself related to the asymmetry of the sonic anemometer. This filter also corresponds well to operational conditions of nacelle lidars, assuming reasonable yaw misalignment of the turbine.
- Lidar LOS availability $> 95\%$, to ensure sufficient amount of data within the averaging period.

The calibration relation to consider is the forced linear regression on binned data (see 3.6.2).

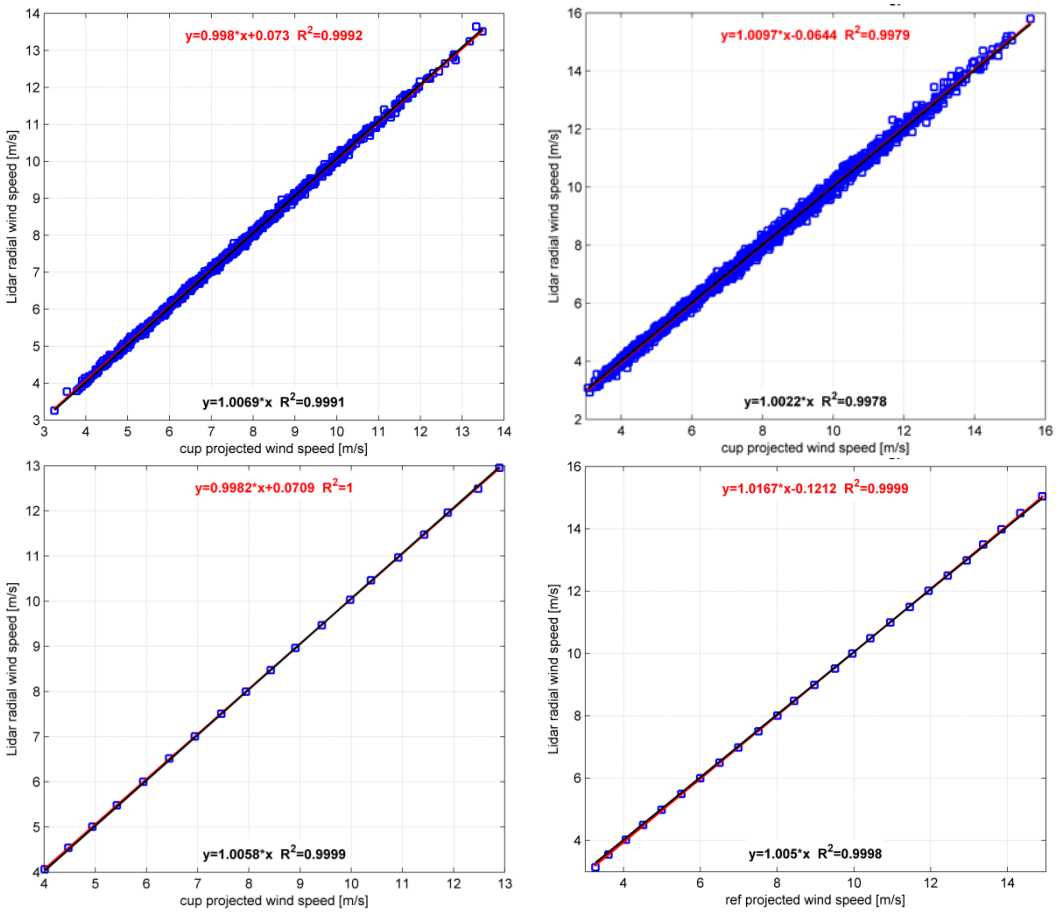

Figure 17. Calibration relation results of the 5-beam Demonstrator (left, LOS0) and ZDM (right) lidars: raw (top) and binned (bottom) data

Each LOS of the 5-beam Demonstrator has been calibrated. For the five forced regressions on binned data, R^2 coefficients are all > 0.9999 and the gains vary between 1.0056 and 1.0090. For ZDM, the narrowest azimuth sector close to the reference instruments (179°-181°) is considered. The forced regression results are: $R^2 = 0.9998$ and $\text{gain} = 1.0050$.

To conclude this section, the feasibility of the white box methodology has been demonstrated through the calibration examples of two different types of profiling nacelle lidars. The calibration results show consistent gains in the forced regression with an error of less than 0.9% for both the ZDM lidar and the five LOS of the Avent lidar. However, the larger variability in the gains and offsets of the free regressions requires further investigation.

It should also be mentioned that it is necessary to obtain a minimum of valid data points in all radial wind speed bins. Practically, filling in all bins depends on wind conditions during the calibration and can therefore be time-consuming. Criteria on the bin validity and number of valid bins should be defined by the accredited laboratory to consider the calibration complete. In the examples of the 5-beam Demonstrator and ZDM lidara, a bin is considered valid if it contains a minimum of three data points.

Chapter 5

5 Measurement uncertainty

Different methods exist to assess measurement uncertainties. They are compiled in metrological standards: e.g. GUM [7], Monte-Carlo [14], bootstrap. The terminology used in this report also refers to metrological vocabulary standards [6].

5.1 Uncertainty definition and types

The VIM [6] defines uncertainty as a "*non-negative parameter characterizing the dispersion of the quantity values being attributed to a measurand, based on the information used*".

In essence, the measured quantity value is only an approximation of the unknowable true value, i.e. the best estimate. The uncertainty of a measured quantity value defines the interval centered on the best estimate and within which the true value lies with a certain probability.

Uncertainty components can be divided in two types (see [6] for definitions): type A are estimated using statistical tools, while type B are estimated by any other means. Type A uncertainties characterize the dispersion of the measurements under defined conditions. In terms of RWS calibration, type A uncertainties correspond to the variability of the lidar measurements under repeatable conditions.

5.2 The question of repeatability

One particularity of field measurements in wind energy is that atmospheric conditions cannot be controlled. Therefore, repeatability does not formally exist. Repeatable conditions could be defined by grouping data according to wind speed, turbulence intensity, temperature, aerosols concentration, thermal stability, etc. Obtaining sufficient calibration datasets under repeatable conditions would require years of measurement data and is consequently not reasonably feasible. Thus, RWS measurement uncertainties cannot be assessed using only statistical methods (type A).

5.3 The GUM method

The GUM methodology steps are:

1) Define the measurement model: $y = f(x_1, x_2, \dots, x_n)$
   where y is the measurement result and $x_1, x_2, \dots, x_n$ are the input quantities
2) List the input quantities and determine their uncertainties
3) Evaluate covariances between input quantities
4) Calculate the measured value y
5) Combine the uncertainty components using the law of propagation of uncertainties
6) Derive and report the expanded uncertainty by multiplying the combined uncertainty by a coverage factor

5.4 RWS uncertainty using GUM

In this paragraph, five different and arbitrarily chosen measurement models are investigated (one in 5.4.1, two in 5.4.2 and two in 5.4.3). The GUM methodology is then applied to each of them. For each method, the three parts of a calibration detailed in 1.3.2 are explicitely given: first the measurement model providing the definition of the measurand; second the derivation of uncertainties based on the measurement model; finally the best estimate relation i.e. how to correct the lidar indicated RWS values.

When used as a stand-alone instrument, the lidar's calibrated measurement will be obtained by correcting the lidar's indicated quantity value with the selected measurement model.

5.4.1 Option 1: lidar-reference measurement error

5.4.1.1 Model definition

In option 1, the estimated measurand y_m is defined using the lidar measurement error ΔRWS:

$$y_m = Ref_{eq\ RWS} + \Delta RWS_i \quad \text{(eq. 6)}$$

where $\Delta RWS_i = \langle\langle RWS_{indicated}\rangle - Ref_{eq\ RWS}\rangle_i$. We also recall here that $Ref_{eq\ RWS}$ corresponds to the 10-min averaged reference quantity value. $\langle\ \ \rangle$ is the time average. $\langle\ \ \rangle_i$ is the average of quantities in bin i.

The input quantities are $Ref_{eq\ RWS}$ and ΔRWS_i. If this model is selected, the RWS calibration report must provide the mean value of the measurement error for each RWS bin in order to correct for the lidar indicated values.

5.4.1.2 Combined uncertainty

Using the law of propagation of uncertainties for correlated input quantities, and since $\frac{\partial(RWS_{BE})}{\partial(Ref_{eq\ RWS})} = \frac{\partial(RWS_{BE})}{\partial(\Delta RWS)} = 1$, we obtain the combined uncertainty on the RWS best estimate:

$$u_{c,y_m} = \sqrt{u^2_{c,Ref_{eq\ RWS}} + s^2_{\Delta RWS} + 2 \cdot cov\left(s_{\Delta RWS}, u_{c,Ref_{eq\ RWS}}\right)} \quad \text{(eq. 7)}$$

where $u_{c,X}$ is the combined uncertainty of X. Provided that a large enough number of data points is obtained for each bin, the covariance can be estimated via the cross-correlation coefficient $\mathrm{r}\left(s_{\Delta RWS}, u_{c,Ref_{eq\ RWS}}\right)$:

$$cov\left(s_{\Delta RWS}, u_{c,Ref_{eq\ RWS}}\right) = u_{c,Ref_{eq\ RWS}} \cdot s_{\Delta RWS} \cdot \mathrm{r}\left(s_{\Delta RWS}, u_{c,Ref_{eq\ RWS}}\right)$$

In the case of the ZDM and 5-beam Demonstrator lidars calibration, the estimated covariance is negligible and negative, i.e. neglecting it is conservative.

The combined uncertainty $u_{c,Ref_{eq\ RWS}}$ is obtained as described in 5.4.4. $s_{\Delta RWS}$ is estimated statistically (**type A**) in each bin:

$$s_{\Delta RWS,i} = \frac{\sigma_{\Delta RWS,i}}{\sqrt{n_i}}$$

where n_i is the number of data point in bin i.

5.4.1.3 Correction of the RWS indication

The lidar best estimate is obtained by finding the bin in which $RWS_{indicated}$ lies and correct it as follows:

$$\langle RWS_{BE} \rangle = \langle RWS_{indicated} \rangle - \Delta RWS_i \quad \text{(eq. 8)}$$

5.4.2 Option 2: forced linear regression(s) between the lidar and reference quantity values

5.4.2.1 Model definition

In option 2, the estimated measurand y_m is defined using the forced linear regressions between the lidar and reference quantity values:

$$y_m = a_{binned} \cdot Ref_{eq\ RWS} \quad \text{(eq. 9)}$$

where a_{binned} is the gain of the forced regression of the binned calibration data (see 3.6.2).

5.4.2.2 Combined uncertainty

Applying the law of propagation of uncertainties for uncorrelated input quantities gives:

$$u_{c,y_m} = \sqrt{{a_{binned}}^2 \cdot u^2_{c,Ref_{eq\ RWS}} + {Ref_{eq\ RWS}}^2 \cdot u^2_{a_{binned}}} \quad \text{(eq. 10)}$$

The uncertainty $u_{a_{binned}}$ can be taken as the half-width of the confidence interval of the gain at 68% (equivalent to a coverage factor of 1). Since the gain $a_{binned} \approx 1$, we can simplify (eq. 7):

$$u_{c,y_m} = \sqrt{u^2_{c,Ref_{eq\ RWS}} + Ref^2_{eq\ RWS} \cdot u^2_{a_{binned}}}$$

5.4.2.3 Correction of the RWS indication

The lidar best estimate is:

$$\langle RWS_{BE} \rangle = \frac{\langle RWS_{indicated} \rangle}{a_{binned}} \quad \text{(eq. 11)}$$

5.4.2.4 Options 2a and 2b

Option 2a here consists in correcting the lidar RWS using the gain of the forced regression of the binned calibration data.

Option 2b is the same as 2a except that the gain used in the measurement model and combined uncertainty is not constant through all bins. Instead, in each bin a forced regression is performed on the 10-minute averaged data, and its gain used:

$$\langle RWS_{BE} \rangle = \frac{\langle RWS_{indicated} \rangle}{a_i}$$

5.4.3 Option 3: unforced linear regression(s) between the lidar and reference quantity values

5.4.3.1 Model definition

In option 3, the estimated measurand y_m is defined using the unforced linear regressions between the lidar and reference quantity values:

$$y_m = a_{binned} \cdot Ref_{eq\ RWS} + b_{binned} \quad \text{(eq. 12)}$$

where a_{binned}, b_{binned} are the gain and offset of the unforced regression of the binned calibration data (see 3.6.2).

5.4.3.2 Combined uncertainty

Applying the law of propagation of uncertainties for uncorrelated input quantities gives:

$$u_{c,y_m} = \sqrt{{a_{binned}}^2 \cdot u^2_{c,Ref_{eq\ RWS}} + {Ref_{eq\ RWS}}^2 \cdot u^2_{a_{binned}} + u^2_{b_{binned}}} \quad \text{(eq. 13)}$$

$u_{a_{binned}}$, $u_{b_{binned}}$ can be taken as the half-width of the confidence intervals at 68%. Note that here a_{binned} is different from 5.4.2.1. Since $a_{binned} \approx 1$ and $b_{binned} \approx 0$ we can simplify (eq. 13):

$$u_{c,y_m} = \sqrt{u^2_{c,Ref_{eq\ RWS}} + u^2_{b_{binned}} + {Ref_{eq\ RWS}}^2 \cdot u^2_{a_{binned}}}$$

5.4.3.3 Correction of the RWS indication

The lidar best estimate is:

$$\langle RWS_{BE} \rangle = \frac{\langle RWS_{indicated} \rangle - b_{binned}}{a_{binned}} \quad \text{(eq. 14)}$$

5.4.3.4 Options 3a and 3b

Options 3a and 3b are similar to options 2a and 2b respectively except that the unforced regression is used instead. For option 3b, in each bin, an unforced linear regression is performed and used:

$$\langle RWS_{BE} \rangle = \frac{\langle RWS_{indicated} \rangle - b_i}{a_i}$$

5.4.4 Combined uncertainty on the reference quantity value

In this section, the reference quantity and calibration process uncertainty sources are given together with the method to assess the combined uncertainty $u_{c,Ref_{eq\ RWS}}$ required to compute the combined RWS uncertainty (eq. 7). The cup and the sonic anemometers will be considered to provide respectively HWS and wind direction reference measurements.

5.4.4.1 Reference instrument(s) uncertainty sources

The HWS uncertainty evaluation follows the IEC 61400-12-1 methodology [12]. It should be mentioned that most of the numeric values used in this methodology are empirical and somewhat arbitrary. In the calibration that has been performed, the HWS uncertainty sources are:

- **Wind tunnel calibration uncertainty (type B):**

$$u_{cal} = u_{cal\,1} + \frac{0.01}{\sqrt{3}} \cdot HWS$$

where $u_{cal\,1}$ ($\approx 0.0255\ m/s$ in section 4) is the uncertainty specified by the calibration certificate for a coverage factor $k = 1$. The 2nd term of u_{cal} is due to the variability of cup anemometers calibration results for Measnet accredited wind tunnels. Measnet states that the tunnels are within $\pm 1\%$. Hence a 1% uncertainty on the HWS is added with an assumed rectangular distribution of uncertainty yielding the $1/\sqrt{3}$ factor.

- **Operational uncertainty (type B):**

$$u_{ope} = \frac{1}{\sqrt{3}} \cdot cup\ class\ number \cdot (0.05 + 0.005 \cdot HWS)$$

The class number of a cup anemometer is an uncertainty component characterising the deviations of measurement values due to environmental conditions, e.g. angular response, turbulence, temperature (influence on bearing friction), etc. The class number of the cup anemometer used during the ZDM and 5-beam Demonstrator lidars is 0.9 (class A).
Note: the class uncertainty can be reduced using a class S corresponding to the wind conditions at the site where the calibration is performed.

- **Mounting uncertainty (type B):**

$$u_{mast} = 0.5\% \cdot HWS$$

Annex G of [12] does not specify uncertainties for top-mounted instruments. However, this may not be realistic, hence the choice to add an arbitrary uncertainty component of 0.5% corresponding to half of the minimum uncertainty for side-mounted instruments.This is also the suggested uncertainty in the revision of the IEC 61400-12-1 currently being implemented (CDV).

The **uncertainty of the wind direction (type B)** measured by the sonic anemometer is taken from the calibration certificate with $k = 1$: $u_{WD} \approx 0.4°$. This choice is due to the lack of standard uncertainty assessment procedures for wind direction measured by sonic anemometers.

5.4.4.2 Calibration process uncertainty sources

Uncertainty sources in the calibration measurement process are:

- **LOS direction uncertainty (type B)** in its evaluation using data analysis (cf. 3.6.1), and roughly estimated to:

$$u_{LOS\,dir} = 0.1°$$

- **Uncertainty of physical inclination angle (type B)** characterising the uncertainty of angle used in the vertical projection of the HWS in (eq. 2) and estimated via the inclinometers'calibration to:

$$u_{\varphi} = 0.05°$$

- **Beam positioning uncertainty (type B)** resulting in wind speed deviations. This component characterises how close to the reference instruments height is the beam position (see 3.2). For example, modelling the vertical shear profile using a power law and shear exponent[7] $\alpha_{exp} = 0.2$, a height uncertainty $u_H = 10\ cm$ at $H = 8.9\ m$, the wind speed uncertainty due to the height error is:

$$u_{pos} = \alpha_{exp} \cdot \frac{u_H}{H} \cdot HWS \approx 0.23\% \cdot HWS$$

- **Inclined beam and range uncertainty (type B)**: practically, the inclined beam implies that the laser light travels, within the probe volume, through a range of heights. The lidar thus senses different wind speeds. Additionally, the range uncertainty along the LOS moves the center of the heights' range slightly away from the reference instruments' height. A model of this uncertainty is detailed in Annex A. This uncertainty depends on:
  - The probe length D_{probe}: for pulsed lidar, D_{probe} is constant; for CW lidars, D_{probe} increases with the measurement range
  - The physical tilting of the beam: $\varphi_{physical} \approx 1.6°$
  - The reference height: $H_{ref} = 8.9m$
  - The range uncertainty: in order to be conservative, we suggest $u_{range} = 5m$
  - The chosen vertical shear profile model: once again, a power law profile and shear exponent of 0.2 is suggested.

  Configuring this model with the 5-beam Demonstrator and ZDM lidars calibration setup in Høvsøre, we obtained $u_{inc,5beam} = 0.052\% \cdot HWS$ and $u_{inc,ZDM} = 0.104\% \cdot HWS$ respectively.

- **Spatial separation uncertainty**: the spatial separation between the two reference sensors infers an uncertainty whose magnitude increases with the separation distance. In our case, the two masts are 5m apart and the terrain is flat. The spatial separation effects can reasonably be neglected. However, one should remember to estimate this uncertainty in the case of larger separations (e.g. 50m).

5.4.4.3 Derivation of the combined uncertainty

The law of propagation of uncertainties is applied to (eq. 2). The calculation details are given in Annex B. It can be demonstrated that the correlation between input quantities are negligible. Thus, using the GUM, the combined uncertainty on the reference quantity value is given by:

$$u^2_{c,Ref_{eq\ RWS}} = \left(\frac{\partial Ref_{eq\ RWS}}{\partial \langle HWS \rangle_{vec}} \cdot u_{c,\langle HWS \rangle_{vec}}\right)^2 + \left(\frac{\partial Ref_{eq\ RWS}}{\partial \langle \varphi_{physical} \rangle} \cdot u_{\langle \varphi_{physical} \rangle}\right)^2 + \left(\frac{\partial Ref_{eq\ RWS}}{\partial (\langle \theta \rangle_{vec} - LOS_{dir})} \cdot u_{c,\langle \theta \rangle_{vec} - LOS_{dir}}\right)^2 \quad \text{(eq. 15)}$$

[7] $\alpha_{exp} = 0.2$ corresponds to typical shear exponent values in flat terrain. In Høvsøre, such a value is conservative since it is usually measured to be lower (~ 0.15).

The partial derivatives, also called sensitivity coefficients are computed for each 10-minute period:

$$\frac{\partial Ref_{eq\,RWS}}{\partial \langle HWS \rangle_{vec}} = \cos\left(\langle \varphi_{physical} \rangle\right) \cdot \cos(\langle \theta \rangle_{vec} - LOS_{dir})$$

$$\frac{\partial Ref_{eq\,RWS}}{\partial \langle \varphi_{physical} \rangle} = -\sin\left(\langle \varphi_{physical} \rangle\right) \cdot \langle HWS \rangle_{vec} \cdot \cos(\langle \theta \rangle_{vec} - LOS_{dir})$$

$$\frac{\partial Ref_{eq\,RWS}}{\partial (\langle \theta \rangle_{vec} - LOS_{dir})} = -\sin(\langle \theta \rangle_{vec} - LOS_{dir}) \cdot \cos\left(\langle \varphi_{physical} \rangle\right) \cdot \langle HWS \rangle_{vec}$$

The individual uncertainties (eq. 15) of the input quantities are computed as follows:

$$u_{c,\langle HWS \rangle_{vec}} = \sqrt{u_{cal}^2 + u_{ope}^2 + u_{mast}^2 + u_{pos}^2 + u_{inc}^2}$$

$$u_{\langle \varphi_{physical} \rangle} = u_{\varphi}$$

$$u_{c,\langle \theta \rangle_{vec} - LOS_{dir}} = \sqrt{u_{WD}^2 + u_{LOS_{dir}}^2}$$

NB: one should remember to convert angle uncertainties to radians when computing the combined uncertainty.

5.5 Binning and expanded RWS uncertainty

The 10-minute data and their uncertainties are binned in the same manner as in 3.6.2. Due to the dependence of the sensitivity coefficients (5.4.4.3) to e.g. wind direction, in terms of reporting, the uncertainty components must be derived for each 10-min period, and then bin-averaged, in order to avoid underestimation. Uncertainty components summed in squares are averaged using the root mean square (e.g. u_{mast}). Uncertainty components resulting from a sum of squares (e.g. $u_{c,\langle HWS \rangle_{vec}}$, u_{c,y_m}) are averaged arithmetically.

Finally, the expanded uncertainty on the estimated measurand y_m is derived, k being the coverage factor:

$$U_{y_m,i} = k \cdot u_{c,\,y_m,i}$$

Usually, the value of $k = 2$ is chosen. In that case, $U_{y_m,i}$ corresponds to the half-width of a 95% confidence interval for a normal probability distribution (if $k = 1 \Leftrightarrow$ 68%; if $k = 3 \Leftrightarrow$ 99%; …).

Note that $u_{c,\,y_m}$ is the final value of the calibration uncertainty for the RWS best estimate (once in the field, there will be additional uncertainty components than the calibration, e.g. flow inhomogeneity in complex terrain).

Figure 18 displays the binned calibration results together with the expanded uncertainty in error bars. In this example, option 1 and 3b are used. Almost no difference exist in the uncertainty results between option 1 and options 2a, 2b or 3a (see Figure 19) due to the large prevalence of the reference quantity uncertainty (see 5.8). Option 3b yields meaningless uncertainty levels because of extreme values of uncertainties on the gain and offset of the unforced regression performed in each bin: the scatter of data in narrow bins induces low-quality linear regressions.

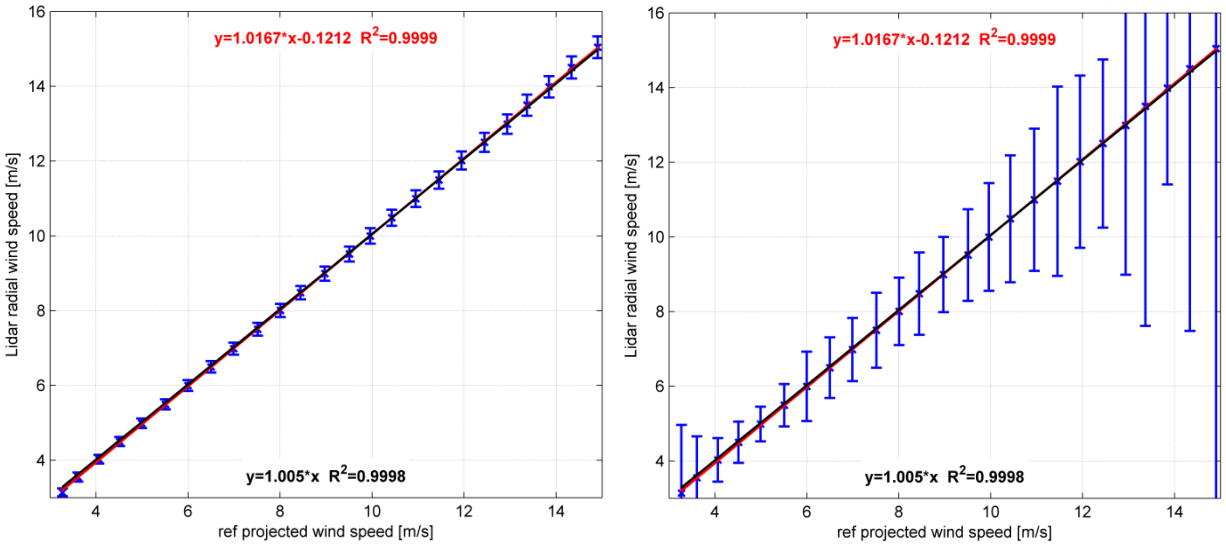

Figure 18. Examples of the calibration uncertainty results: expanded uncertainty shown in error bars (left: option 1; right: option 3b)

5.6 Reconstructed parameter uncertainty assessment

The ultimate goal of the white box methodology is to derive uncertainties on reconstructed parameters using the RWS uncertainty and the reconstruction algorithms. If the GUM methodology is used, the cross-correlation between all inputs of the algorithm must also be estimated.

The reconstructed parameter(s) uncertainty assessment is specific to one type of lidar and will therefore not be detailed in this report. An example of such an uncertainty assessment is given in [13] for the HWS reconstructed using a two-beam nacelle lidar and the GUM methodology [7]. Examples are also introduced in [9] and [10].

5.7 Which calibration relation to apply to the lidar RWS?

For reasons explained in 5.5, option 3b will not be considered. The obtained uncertainties are compared for all the other options.

Figure 19 displays the uncertainty results for these four options 1, 2a, 2b and 3a. Uncertainties are expressed in [m/s] and [%] of the RWS bin center (equals to half of the bin number), respectively for the top and bottom graphs. It can be observed that all options give very similar expanded uncertainty values of approximately 2-3%. The absolute uncertainty values vary linearly with the wind speed, suggesting that one uncertainty component prevails and is proportional to the wind speed.

Despite their similarity, one of the 4 proposed measurement models must be selected. The selection criteria can also be qualitative. First, we must mention that options 1 and 2b can create gaps and overlaps in the corrected measurand (the best estimate), i.e. depending on the ΔRWS_i or a_i values some ranges of RWS might never be obtained[8]. Atmospheric winds do not feature such gaps. Hence, even though the simplicity of

[8] For example, using option1:
- if $\langle RWS_{indicated} \rangle = 5.74\ m/s$ is corrected with $\Delta RWS_i = 0.05\ m/s$, $\langle RWS_{BE} \rangle = 5{,}69\, m/s$
- if $\langle RWS_{indicated} \rangle = 5.76\ m/s$ is corrected with $\Delta RWS_{i+1} = -0.10\ m/s$, $\langle RWS_{BE} \rangle = 5{,}86\, m/s$

In such a situation, values in the $[5.70\ ;\ 5.80]\ m/s$ range cannot be obtained.

option 1 is attractive, options 2a and 3a are preferred. The only remaining criterion is the physics of lidars, which suggest that there should not be a significant offset.

The author's advice is to **select option 2a.** Alternatively, option 3a can be selected when the offset value of the unforced linear regression is significant.

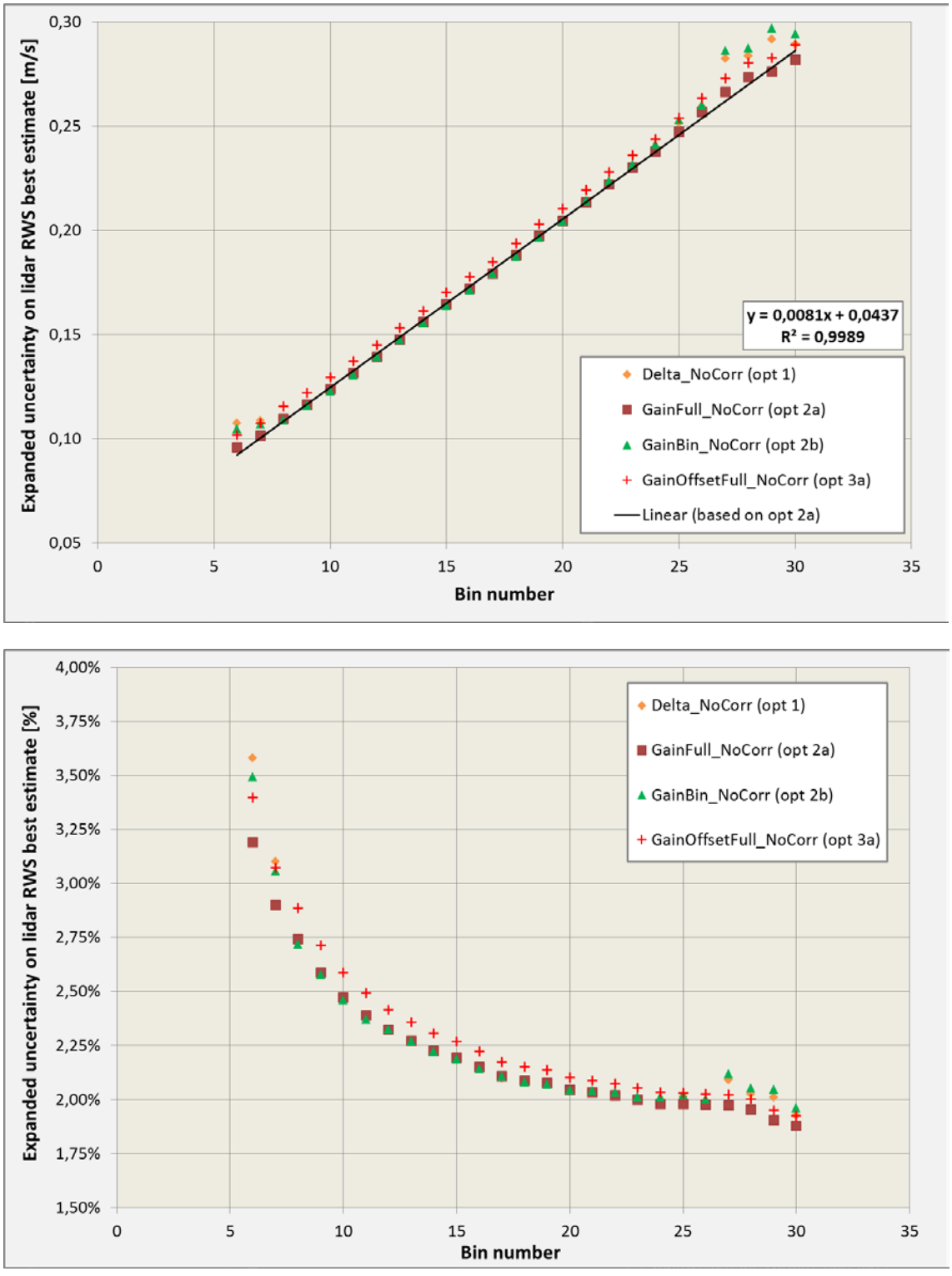

Figure 19. Comparison of uncertainty results vs. measurement model: top [m/s], bottom [% RWS]

5.8 Prevailing uncertainty sources

Identifying the prevailing uncertainty sources is essential to assess the quality of the calibration process and to show the way forward to substantially reduce wind measurement uncertainties. This analysis is performed through the example of option 2a.

5.8.1 Tables of uncertainty components

Option 2a is analysed further:

- Table 1[9] shows that ~99% of u_{c,y_m}– the uncertainty on the measurand estimated using the measurement model (eq. 10) – is related to the reference quantity value (columns 8-10). In addition, the HWS measured by the cup anemometer contributes for over 90% to $u_{c,Ref_{eq\ RWS}}$ (columns 4-7), even though $u_{c,\langle HWS\rangle_{vec}}$ is weighed by the cosines of both the vertical and horizontal projection angles.
- The main contribution to $u_{c,\langle HWS\rangle_{vec}}$ are the calibration, operational and mounting uncertainties (Table 2). These three components contribute for ~90% to the horizontal wind speed uncertainty.

Table 1. Partial uncertainty results (option 2a) for y_m and $Ref_{eq\ RWS}$

1	2	3	4	5	6	7	8	9	10
Bin	Lower RWS	Upper RWS	U HWS to ref	U tilt to ref	U Wdrel to ref	Uc ref	U ym ref	U ym gain	Uc ym
-	[m/s]	[m/s]	[m/s]	[m/s]	[m/s]	[m/s]	[m/s]	[m/s]	[m/s]
…	…	…	…	…	…	…	…	…	…
10	4,75	5,25	0,0596	0,0001	0,0143	0,0613	0,0616	0,0056	0,0618
11	5,25	5,75	0,0635	0,0001	0,0146	0,0651	0,0654	0,0062	0,0657
12	5,75	6,25	0,0669	0,0002	0,0172	0,0690	0,0694	0,0067	0,0697
…	…	…	…	…	…	…	…	…	…
25	12,25	12,75	0,1175	0,0003	0,0340	0,1223	0,1230	0,0139	0,1237
26	12,75	13,25	0,1214	0,0003	0,0371	0,1269	0,1276	0,0145	0,1284
…	…	…	…	…	…	…	…	…	…

[9] For convenience, the uncertainty results are presented partially. See Annex E for the complete tables.

Table 2. Partial uncertainty results (option 2a) for $\langle HWS \rangle_{vec}$

1	2	3	4	5	6	7	8	9
Bin	Lower RWS	Upper RWS	U cal tot	U ope tot	U mast	U pos	U inc	Uc HWS
-	[m/s]	[m/s]	[m/s]	[m/s]	[m/s]	[m/s]	[m/s]	[m/s]
…	…	…	…	…	…	…	…	…
10	4,75	5,25	0,0399	0,0399	0,0269	0,0124	0,0056	0,0639
11	5,25	5,75	0,0421	0,0412	0,0294	0,0135	0,0061	0,0674
12	5,75	6,25	0,0449	0,0427	0,0323	0,0148	0,0067	0,0717
…	…	…	…	…	…	…	…	…
25	12,25	12,75	0,0810	0,0606	0,0666	0,0306	0,0138	0,1255
26	12,75	13,25	0,0844	0,0622	0,0697	0,0321	0,0145	0,1306
…	…	…	…	…	…	…	…	…

5.8.2 "Tree structure" of uncertainties and contribution to total combined RWS uncertainty

The relative importance of uncertainty components can be visualised by plotting their cumulated sum of squares[10]. Figure 20 and Figure 21 show the results respectively for $u_{c,Ref_{eq\ RWS}}$ and $u_{c,\langle HWS \rangle_{vec}}$.

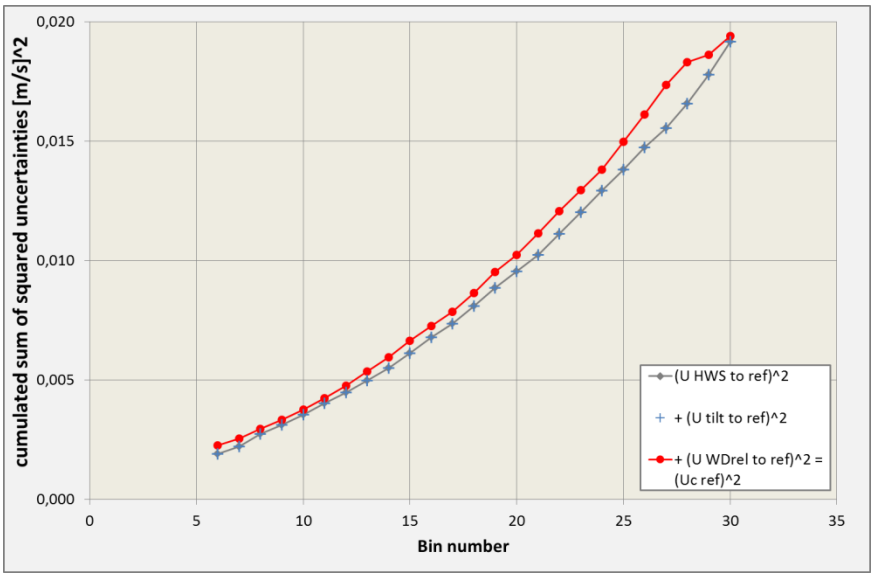

Figure 20. Cumulated sum of squared uncertainty components contributing to $u_{c,Ref_{eq\ RWS}}$

[10] e.g. to analyse $u_{c,\langle HWS \rangle_{vec}}$, one can successively plot u_{cal}^2, $\left(u_{cal}^2 + u_{ope}^2\right)$, …, $\left(u_{cal}^2 + u_{ope}^2 + u_{mast}^2 + u_{pos}^2 + u_{inc}^2\right)$.

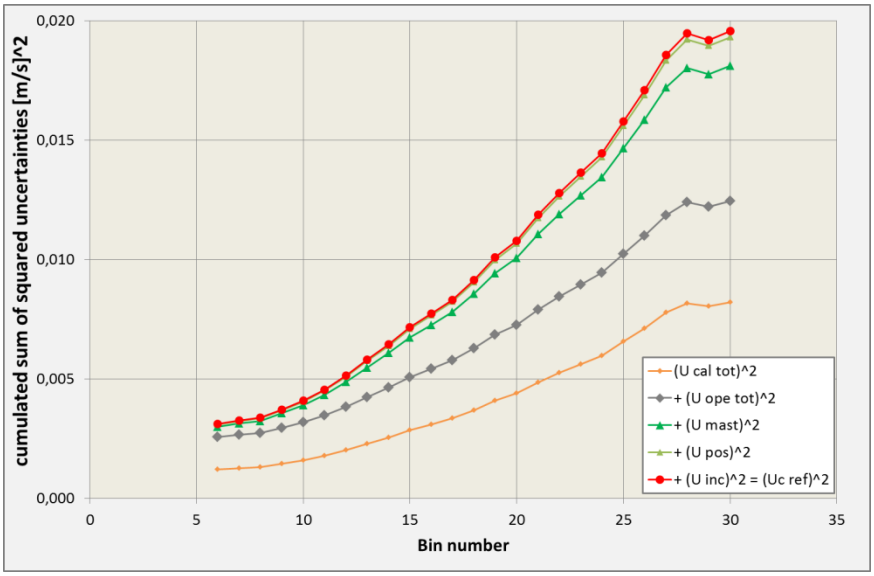

Figure 21. Cumulated sum of squared uncertainty components contributing to $u_{c,\langle HWS\rangle_{vec}}$

The relative importance of each uncertainty component can alternatively be visualised in the form of a "tree structure" (see Figure 22). The percentages are the average contribution of each uncertainty component to the combined uncertainty of the next "level". Each level is represented in one colour.

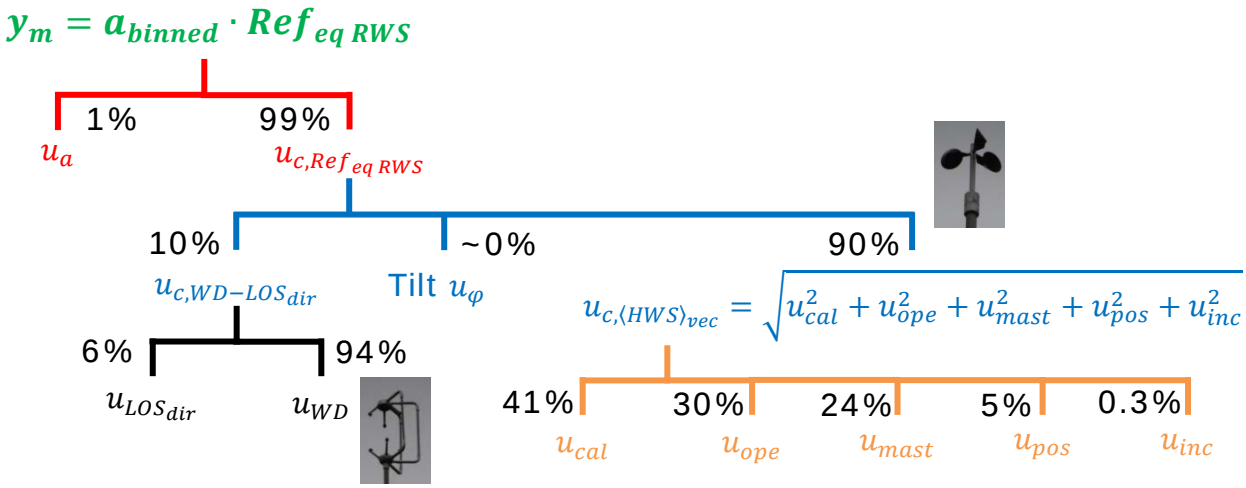

Figure 22. « Tree structure » of uncertainties using option 2a: contribution of uncertainty components to combined uncertainties

The uncertainties related to the RWS calibration procedure ($u_{LOS_{dir}}$, u_{pos}, u_{inc}, u_φ, u_a) seldom contribute to the combined uncertainty on the lidar's RWS best estimate, therefore demonstrating the quality of the procedure.

The analysis also points out the weaknesses of the HWS reference instrument calibration. The mounting uncertainty is added arbitrarily, while the calibration and operational uncertainties are where efforts should be made to reduce the horizontal wind speed combined uncertainty. In particular, the spread in Measnet accredited wind tunnels could be avoided with better cup calibration procedures.

5.9 Should the lidar indications be corrected?

Lidars are currently calibrated in uncontrolled conditions (temperature, turbulence, etc). Cup anemometers – commonly used for wind speed measurements – respond differently to these external variables, which makes the calibration specific to those conditions.

The GUM clearly states that known systematic effects should always be corrected for (see 6.3.1. in [7]) except in special cases (see F2.4.5 in [7]). The RWS calibration of nacelle lidars does not comply with the criteria corresponding to such a situation.

The white box method implies that the LOS velocity must be corrected before applying the reconstruction algorithms. Particularly for advanced reconstruction algorithms (e.g. using fitting or recursive techniques), applying such a correction by post-processing the reconstructed data is not feasible. One solution to this problem is that lidars manufacturers allow, in future development of the softwares, to specify the correction to apply to the LOS velocities.

According to the GUM, in the case where the correction of a known systematic effect is not applied, the uncertainties should be enlarged. Following the GUM's recommendations, for nacelle lidars calibration (opt 2a, see 5.4.2), the uncertainty artificially added to the combined uncertainty $u_{c,Ref_{eq\,RWS}}$ could be:

$$bin\ center \cdot (a_{binned} - 1)$$

For example, at 6 m/s and with the derived gain of 1.005, the additional uncertainty is $0.03\ m/s$, i.e. corresponding to over 40% of the combined uncertainty. **Our recommendation is therefore to correct the lidar indications of the RWS measurements**.

Finally, in the examples of the 5-beam Demonstrator and ZDM lidars, the calibration has been performed at a range close the maximum measurement capabilities of both systems. No significant differences in the RWS indications are expected at shorter range because:

- For the 5-beam Demonstrator, the probe length is independent of range. The main difference lies in the higher CNR levels close to the focus point of the beam.
- For the ZDM lidar, the probe length is proportional to the square of the range. Thus, the shorter the range the lower potential deviations and uncertainties are.

Practically, at shorter ranges, the applied LOS velocity corrections and corresponding uncertainties will be the same as long as there is no marked dependence of the RWS to CNR.

Discussion

Previous studies on the calibration of two-beam nacelle lidars have shown that calibrating the inputs of the reconstruction algorithms of lidars was possible. The studies also demonstrated that the radial wind speed (RWS) field calibration provides consistent results. However, the procedures were specific to two-beam pulsed nacelle lidars. They therefore needed adaptation in order to be applicable to any lidar type – laser light type and geometry of scanning pattern – and become generic.

This report identified and detailed two different possible calibration concepts for nacelle-based profiling wind lidars. The retained approach is the radial wind speed calibration – also called white box calibration – which allows estimation of uncertainties of any reconstructed parameter using the derived radial wind speed uncertainties.

Because of their measurement principles, all Doppler wind lidars first estimate the radial wind speed and then use it for wind field reconstruction. Consequently, the radial wind speed calibration is generic in opposition to the black box methodology, which is specific to each reconstructed parameter. This method may provide the scientific basis for implementing standardised calibration procedures for nacelle lidars.

The calibration procedure has been examplified through its application to both a pulsed multi-beam lidar and a continuous wave lidar. Calibrations results from both lidars have proven to be consistent, with a high level of agreement between the measured radial wind speed and reference quantity values, thus confirming the feasibility of the radial wind speed calibration.

However, some limitations must be mentioned. First, the uncertainty components from the reference instrument prevail, emphasizing the need for better calibration procedures for cup anemometers. Second, the measurement setup is not ideal as measuring at low height above ground implies high turbulence intensity. On the other hand, a tall mast would require installing the lidar on an expensive stiff platform to avoid adding measurement uncertainties. Finally, in the white box calibration, having access to reconstruction algorithms is mandatory. These algorithms would need to be provided to the accredited calibration laboratories under confidentiality agreements.

Further work might involve sensitivity analysis of the radial wind speed calibration results to e.g. atmospheric parameters or quantity of valid measurement data. After defining new custom reconstruction algorithms, uncertainties will be derived on the reconstructed outputs. Alternative uncertainty estimation methods to the GUM such as Monte-Carlo may also be investigated.

A controversial question remains: should the lidar measurements be corrected using the calibration results? Although the VIM provides a clear definition of the calibration and formally requires to apply the calibration relation (i.e. correct the measurements), lidars are currently calibrated in uncontrolled conditions (temperature, turbulence, etc). In specific cases where lidars operate in conditions far from those during the calibration, correcting lidar's measurements is not always advisable and artificially enlarging the uncertainties may be preferred. By default, our recommendation remains to follow metrological standards and thus correct lidar measurements.

Annexes

Annex A. Model of bias due to vertical shear within a lidar probe volume and to range error

1. Model of bias due to vertical shear – no range error

This annex shows the influence of the vertical shear within the probe volume of a lidar. Indeed, when the lidar beam is tilted up or down, the probe volume of the lidar is contained within a range of heights $[H_{min}; H_{max}]$.

A simple model of this effect is derived to quantify the introduced bias $error_{shear}$:

$$error_{shear} = \frac{1}{H_{ref}} \cdot \int_{H_{min}}^{H_{max}} \left(V(H) - V_{ref}\right) \cdot dH$$

Where:

- H refers to the height above ground level (a.g.l.)
- H_{ref} is the height a.g.l. of the reference instrument
- $V(H)$ is the horizontal wind speed at H, defined by a chosen model of vertical shear
- V_{ref} is the horizontal wind speed at H_{ref}

The model assumes that the weighing function within the probe volume is uniform (conservative hypothesis), i.e. the lidar does not make a difference between the wind sensed at the centre of the probe volume, or its extremities. If the horizontal distance D_{hor} between the lidar and the reference instrument is fixed, then the physical inclination angle is $\varphi_{physical} = \text{atan}\left(\frac{H_{ref} - H_{lidar}}{D_{hor}}\right)$.

We first assume that the lidar's measurement range corresponds exactly to the reference instrument's height, i.e. the center of the probe volume is located at H_{ref}. With the probe length D_{probe}, we derive:

$$\begin{cases} H_{min} = H_{ref} - D_{probe} \cdot \sin\varphi_{physical} \\ H_{max} = H_{ref} + D_{probe} \cdot \sin\varphi_{physical} \end{cases}$$

Using a **linear shear profile** $V(H) = V_{ref} + gain \cdot \left(H - H_{ref}\right)$, it can be demonstrated that no bias is introduced since the higher wind sensed at H_{max} is exactly balanced by the wind sensed at H_{min}. In other words: $error_{shear}(linear) = 0\ m/s$.

Using a **"power law" shear profile** with the exponent α_{exp}, we have:

$$V(H) = V_{ref} \cdot \left(\frac{H}{H_{ref}}\right)^{\alpha_{exp}}$$

This shear profile further leads to a bias (in m/s):

$$\begin{aligned} error_{shear}(power\ law) &= \frac{V_{ref}}{H_{ref}} \cdot \left(\frac{H_{max}^{\alpha_{exp}+1} - H_{min}^{\alpha_{exp}+1}}{(\alpha_{exp}+1) \cdot H_{ref}^{\alpha_{exp}}} - H_{max} + H_{min}\right) \\ &= \frac{V_{ref}}{H_{ref}} \cdot \left(\frac{H_{max}^{\alpha_{exp}+1} - H_{min}^{\alpha_{exp}+1}}{(\alpha_{exp}+1) \cdot H_{ref}^{\alpha_{exp}}} - 2D_{probe} \cdot \sin\varphi_{physical}\right) \end{aligned} \quad \text{(eq. 16)}$$

Dividing $error_{shear}$ by V_{ref}, one can observe the relative error does not depend on the horizontal wind speed, but only on the measurement height, the physical inclination of the beam, and on the shear exponent. The table below shows a matrix of relative $error_{shear}$ calculated for a fixed shear profile ($\alpha_{exp} = 0.2$) and variable H_{ref} and $\varphi_{physical}$, and probe length $D_{probe} = 25m$ (i.e. the probe length of the 5-beam Demonstrator lidar).

Table 3. Wind speed uncertainty due to vertical shear (type 'power law', exponent $\alpha_{exp} = 0.2$) within a lidar probe volume of length $D_{probe} = 25m$

		physical beam inclination (°)										
		0	1	2	3	4	5	10	15	20	25	30
measurement height Href (m)	5	0,000%	-0,003%	-0,028%	-0,094%	-0,227%	-0,450%	-4,382%	#NUM!	#NUM!	#NUM!	#NUM!
	10	0,000%	0,000%	-0,003%	-0,012%	-0,028%	-0,054%	-0,445%	-1,581%	-4,138%	#NUM!	#NUM!
	20	0,000%	0,000%	0,000%	-0,001%	-0,003%	-0,007%	-0,054%	-0,180%	-0,424%	-0,823%	-1,411%
	30	0,000%	0,000%	0,000%	0,000%	-0,001%	-0,002%	-0,016%	-0,053%	-0,122%	-0,233%	-0,392%
	40	0,000%	0,000%	0,000%	0,000%	0,000%	-0,001%	-0,007%	-0,022%	-0,051%	-0,097%	-0,162%
	50	0,000%	0,000%	0,000%	0,000%	0,000%	0,000%	-0,003%	-0,011%	-0,026%	-0,049%	-0,082%
	60	0,000%	0,000%	0,000%	0,000%	0,000%	0,000%	-0,002%	-0,007%	-0,015%	-0,028%	-0,047%
	70	0,000%	0,000%	0,000%	0,000%	0,000%	0,000%	-0,001%	-0,004%	-0,009%	-0,018%	-0,030%
	80	0,000%	0,000%	0,000%	0,000%	0,000%	0,000%	-0,001%	-0,003%	-0,006%	-0,012%	-0,020%
	90	0,000%	0,000%	0,000%	0,000%	0,000%	0,000%	-0,001%	-0,002%	-0,004%	-0,008%	-0,014%
	100	0,000%	0,000%	0,000%	0,000%	0,000%	0,000%	0,000%	-0,001%	-0,003%	-0,006%	-0,010%

In Table 3, red/green cells correspond to bias greater/less than 0.01% of V_{ref}. This model shows that introduced biases would still be negligible with a large inclination angle as long as the measurement height is sufficient. However, with greater heights come other measurement error sources such as the tilting of the reference mast.

Note: with a 262m range and $\varphi_{physical} = 1.6°$, the model shows that the relative bias due to the inclined beam is:

- for the 5-beam Demonstrator lidar, -0.003%.
- for the ZDM lidar, -0.015% ($D_{probe} = 44.7m$).

2. Model of bias due to vertical shear and range error

With no measurement range error, it has been demonstrated that the bias due to shear within an inclined probe volume is negligible. The reason is the compensation between winds sensed at greater and lower heights. However, if a range error (e.g. misconfiguratiom) or a range uncertainty (u_{range}) is included, the interval $[H_{min}; H_{max}]$ is not centered on H_{ref} anymore:

$$\begin{cases} H_{min} = H_{ref} + \left(u_{range} - D_{probe}\right) \cdot \sin \varphi_{physical} \\ H_{max} = H_{ref} + \left(u_{range} + D_{probe}\right) \cdot \sin \varphi_{physical} \end{cases} \quad \text{(eq. 17)}$$

a. Linear shear profile

A linear shear profile gives:

$$error_{shear}(linear\ shear) = gain \cdot \left(\frac{H_{max}^2 - H_{min}^2}{2 \cdot H_{ref}} - (H_{max} - H_{min}) \right)$$
$$= -2 \cdot gain \cdot \frac{u_{range} \cdot D_{probe} \cdot \sin \varphi_{physical}{}^2}{H_{ref}}$$

b. Power law shear profile

With a power law shear profile, $\text{error}_{\text{shear}}$ is derived using (eq. 16) and (eq. 17). Depending on whether u_{range} is added or substracted in (eq. 17), $error_{shear}$ can take two different values. The HWS uncertainty due to vertical shear and range uncertainty is the maximum of the two solutions.

Table 4 shows the results for the 5-beam Demonstrator lidar. Table 5 shows the results for the ZDM lidar at a measurement distance of 262m corresponding to a probe length of 45m. Both tables are given for $u_{range} = 5m$.

Table 4. Wind speed uncertainty due to vertical shear (type 'power law', exponent $\alpha_{exp} = 0.2$) within a lidar probe volume and to a 5m range uncertainty – $D_{probe} = 25m$ (5-beam Demonstrator lidar)

		physical beam inclination (°)										
		0	1,6	2	3	4	5	10	15	20	25	30
measurement height Href (m)	5	0,000%	0,171%	0,274%	0,658%	1,251%	2,096%	#NUM!	#NUM!	#NUM!	#NUM!	#NUM!
	8,9	0,000%	0,052%	0,082%	0,191%	0,351%	0,569%	2,745%	7,816%	#NUM!	#NUM!	#NUM!
	20	0,000%	0,010%	0,016%	0,036%	0,064%	0,102%	0,438%	1,055%	2,003%	3,338%	5,132%
	30	0,000%	0,004%	0,007%	0,016%	0,028%	0,044%	0,184%	0,432%	0,795%	1,279%	1,886%
	40	0,000%	0,002%	0,004%	0,009%	0,016%	0,024%	0,101%	0,233%	0,424%	0,672%	0,976%
	50	0,000%	0,002%	0,002%	0,006%	0,010%	0,016%	0,064%	0,146%	0,263%	0,413%	0,595%
	60	0,000%	0,001%	0,002%	0,004%	0,007%	0,011%	0,044%	0,100%	0,179%	0,280%	0,401%
	70	0,000%	0,001%	0,001%	0,003%	0,005%	0,008%	0,032%	0,072%	0,129%	0,202%	0,288%
	80	0,000%	0,001%	0,001%	0,002%	0,004%	0,006%	0,024%	0,055%	0,098%	0,152%	0,217%
	90	0,000%	0,000%	0,001%	0,002%	0,003%	0,005%	0,019%	0,043%	0,077%	0,119%	0,169%
	100	0,000%	0,000%	0,001%	0,001%	0,002%	0,004%	0,015%	0,035%	0,062%	0,096%	0,136%

Table 5. Wind speed uncertainty due to vertical shear (type 'power law', exponent $\alpha_{exp} = 0.2$) within a lidar probe volume and to the range uncertainty – $D_{probe} = 45m$ (ZDM lidar)

		physical beam inclination (°)										
		0	1,6	2	3	4	5	10	15	20	25	30
measurement height Href (m)	5	0,000%	0,371%	0,619%	1,644%	3,475%	6,642%	#NUM!	#NUM!	#NUM!	#NUM!	#NUM!
	8,9	0,000%	0,104%	0,169%	0,417%	0,813%	1,393%	9,826%	#NUM!	#NUM!	#NUM!	#NUM!
	20	0,000%	0,019%	0,030%	0,070%	0,131%	0,213%	1,039%	2,838%	6,256%	#NUM!	#NUM!
	30	0,000%	0,008%	0,013%	0,030%	0,055%	0,088%	0,402%	1,023%	2,040%	3,568%	5,781%
	40	0,000%	0,005%	0,007%	0,016%	0,030%	0,048%	0,211%	0,519%	1,001%	1,683%	2,590%
	50	0,000%	0,003%	0,005%	0,010%	0,019%	0,030%	0,129%	0,312%	0,591%	0,974%	1,467%
	60	0,000%	0,002%	0,003%	0,007%	0,013%	0,020%	0,087%	0,208%	0,388%	0,632%	0,941%
	70	0,000%	0,001%	0,002%	0,005%	0,009%	0,015%	0,063%	0,148%	0,274%	0,443%	0,654%
	80	0,000%	0,001%	0,002%	0,004%	0,007%	0,011%	0,047%	0,111%	0,204%	0,327%	0,479%
	90	0,000%	0,001%	0,001%	0,003%	0,006%	0,009%	0,037%	0,086%	0,157%	0,251%	0,366%
	100	0,000%	0,001%	0,001%	0,003%	0,005%	0,007%	0,030%	0,069%	0,125%	0,199%	0,289%

Thus, the inclined beam and range combined uncertainty (see 5.4.4.2) corresponding to the RWS calibration setup in Høvsøre, and expressed in % of the horizontal wind speed, is:

- For the 5-beam Demonstrator lidar: $u_{inc} = 0.052\%$
- For the ZDM lidar: $u_{inc} = 0.104\%$

Annex B. Applying the GUM method to the reference equivalent RWS

This annex provides the mathematical developments to derive the combined uncertainty on the reference quantity value $Ref_{eq\ RWS}$. It employs the same notations as used in this report.

The measurement model of $Ref_{eq\ RWS}$ is given by (eq. 2). Thus, applying the law of propagation of uncertainties first for correlated input quantities yields:

$$u^2_{c,Ref_{eq\ RWS}} = \sum_{j=1}^{6} A_j$$

The six components A_j are given in the following table:

$$A_1 = \left(\frac{\partial Ref_{eq\ RWS}}{\partial \langle HWS\rangle_{vec}} \cdot u_{c,\langle HWS\rangle_{vec}}\right)^2 = \left(\cos\left(\langle\varphi_{physical}\rangle\right) \cdot \cos(\langle\theta\rangle_{vec} - LOS_{dir}) \cdot u_{c,\langle HWS\rangle_{vec}}\right)^2$$

$$A_2 = \left(\frac{\partial Ref_{eq\ RWS}}{\partial \langle\varphi_{physical}\rangle} \cdot u_{\langle\varphi_{physical}\rangle}\right)^2 = \left(-\sin\left(\langle\varphi_{physical}\rangle\right) \cdot \langle HWS\rangle_{vec} \cdot \cos(\langle\theta\rangle_{vec} - LOS_{dir}) \cdot u_{\varphi_{physical}}\right)^2$$

$$A_3 = \left(\frac{\partial Ref_{eq\ RWS}}{\partial \langle\theta\rangle_{vec}} \cdot u_{\langle\theta\rangle_{vec}}\right)^2 + \left(\frac{\partial Ref_{eq\ RWS}}{\partial LOS_{dir}} \cdot u_{LOS_{dir}}\right)^2 = \left(-\sin(\langle\theta\rangle_{vec} - LOS_{dir}) \cdot \cos\left(\langle\varphi_{physical}\rangle\right) \cdot \langle HWS\rangle_{vec}\right)^2 \cdot \left(u^2_{\langle\theta\rangle_{vec}} + u^2_{LOS_{dir}}\right)$$

$$A_4 = 2 \cdot \frac{\partial Ref_{eq\ RWS}}{\partial \langle HWS\rangle_{vec}} \cdot \frac{\partial Ref_{eq\ RWS}}{\partial \langle\varphi_{physical}\rangle} \cdot cov\left(u_{c,\langle HWS\rangle_{vec}}, u_{\langle\varphi_{physical}\rangle}\right) = -2\sin\left(\langle\varphi_{physical}\rangle\right) \cdot \cos\left(\langle\varphi_{physical}\rangle\right) \cdot \cos^2(\langle\theta\rangle_{vec} - LOS_{dir}) \cdot \langle HWS\rangle_{vec} \cdot cov\left(u_{c,\langle HWS\rangle_{vec}}, u_{\langle\varphi_{physical}\rangle}\right)$$

$$A_5 = 2 \cdot \frac{\partial Ref_{eq\ RWS}}{\partial \langle HWS\rangle_{vec}} \cdot \frac{\partial Ref_{eq\ RWS}}{\partial \langle\theta\rangle_{vec}} \cdot cov\left(u_{c,\langle HWS\rangle_{vec}}, u_{\langle\theta\rangle_{vec}}\right) = -2\sin(\langle\theta\rangle_{vec} - LOS_{dir}) \cdot \cos(\langle\theta\rangle_{vec} - LOS_{dir}) \cdot \cos^2\left(\langle\varphi_{physical}\rangle\right) \cdot \langle HWS\rangle_{vec} \cdot cov\left(u_{c,\langle HWS\rangle_{vec}}, u_{\langle\theta\rangle_{vec}}\right)$$

$$A_6 = 2 \cdot \frac{\partial Ref_{eq\ RWS}}{\partial \langle\varphi_{physical}\rangle} \cdot \frac{\partial Ref_{eq\ RWS}}{\partial \langle\theta\rangle_{vec}} \cdot cov\left(u_{\langle\varphi_{physical}\rangle}, u_{\langle\theta\rangle_{vec}}\right) = 2 \cdot \langle HWS\rangle^2_{vec} \cdot \sin(\langle\theta\rangle_{vec} - LOS_{dir}) \cdot \cos(\langle\theta\rangle_{vec} - LOS_{dir}) \cdot \sin\left(\langle\varphi_{physical}\rangle\right) \cdot \cos\left(\langle\varphi_{physical}\rangle\right) \cdot cov\left(u_{\langle\varphi_{physical}\rangle}, u_{\langle\theta\rangle_{vec}}\right)$$

$u_{\langle\varphi_{physical}\rangle}$ and $u_{\langle\theta\rangle_{vec}}$ are constant values. Their covariance with any other input quantity is 0. Thus, $A_4 = A_5 = A_6 = 0$. Therefore, the combined uncertainty will be obtained using uncorrelated input quantities.

Annex C. RWS calibration uncertainty results using option 2a

Table 6. RWS calibration uncertainty results (option 2a) for y_m and $Ref_{eq\ RWS}$

Bin	Lower RWS	Upper RWS	U HWS to ref	U tilt to ref	U Wdrel to ref	Uc ref	U ym ref	U ym gain	Uc ym
-	[m/s]	[m/s]	[m/s]	[m/s]	[m/s]	[m/s]	[m/s]	[m/s]	[m/s]
6	2,75	3,25	0,0436	0,0001	0,0188	0,0475	0,0477	0,0037	0,0479
7	3,25	3,75	0,0471	0,0001	0,0179	0,0504	0,0506	0,0040	0,0508
8	3,75	4,25	0,0524	0,0001	0,0144	0,0544	0,0546	0,0045	0,0548
9	4,25	4,75	0,0558	0,0001	0,0146	0,0577	0,0580	0,0050	0,0582
10	4,75	5,25	0,0596	0,0001	0,0143	0,0613	0,0616	0,0056	0,0618
11	5,25	5,75	0,0635	0,0001	0,0146	0,0651	0,0654	0,0062	0,0657
12	5,75	6,25	0,0669	0,0002	0,0172	0,0690	0,0694	0,0067	0,0697
13	6,25	6,75	0,0705	0,0002	0,0196	0,0731	0,0735	0,0073	0,0738
14	6,75	7,25	0,0742	0,0002	0,0212	0,0771	0,0776	0,0078	0,0779
15	7,25	7,75	0,0782	0,0002	0,0228	0,0814	0,0819	0,0084	0,0823
16	7,75	8,25	0,0823	0,0002	0,0220	0,0852	0,0856	0,0090	0,0860
17	8,25	8,75	0,0858	0,0002	0,0221	0,0886	0,0891	0,0094	0,0895
18	8,75	9,25	0,0899	0,0002	0,0237	0,0930	0,0935	0,0100	0,0940
19	9,25	9,75	0,0940	0,0002	0,0260	0,0975	0,0981	0,0106	0,0986
20	9,75	10,25	0,0978	0,0003	0,0261	0,1011	0,1017	0,0111	0,1022
21	10,25	10,75	0,1012	0,0003	0,0301	0,1055	0,1061	0,0117	0,1067
22	10,75	11,25	0,1054	0,0003	0,0307	0,1098	0,1104	0,0122	0,1110
23	11,25	11,75	0,1096	0,0003	0,0304	0,1137	0,1143	0,0128	0,1150
24	11,75	12,25	0,1137	0,0003	0,0298	0,1174	0,1181	0,0133	0,1188
25	12,25	12,75	0,1175	0,0003	0,0340	0,1223	0,1230	0,0139	0,1237
26	12,75	13,25	0,1214	0,0003	0,0371	0,1269	0,1276	0,0145	0,1284
27	13,25	13,75	0,1247	0,0003	0,0425	0,1316	0,1324	0,0149	0,1331
28	13,75	14,25	0,1287	0,0003	0,0417	0,1352	0,1360	0,0155	0,1368
29	14,25	14,75	0,1334	0,0004	0,0288	0,1364	0,1371	0,0160	0,1380
30	14,75	15,25	0,1384	0,0004	0,0151	0,1392	0,1400	0,0167	0,1409

Table 7. RWS calibration uncertainty results (option 2a) for $\langle HWS \rangle_{vec}$

Bin	Lower RWS	Upper RWS	U cal tot	U ope tot	U mast	U pos	U inc	Uc HWS
-	[m/s]	[m/s]	[m/s]	[m/s]	[m/s]	[m/s]	[m/s]	[m/s]
6	2,75	3,25	0,0348	0,0369	0,0209	0,0096	0,0044	0,0558
7	3,25	3,75	0,0356	0,0374	0,0219	0,0101	0,0046	0,0571
8	3,75	4,25	0,0362	0,0377	0,0226	0,0104	0,0047	0,0580
9	4,25	4,75	0,0380	0,0388	0,0247	0,0114	0,0051	0,0609
10	4,75	5,25	0,0399	0,0399	0,0269	0,0124	0,0056	0,0639
11	5,25	5,75	0,0421	0,0412	0,0294	0,0135	0,0061	0,0674
12	5,75	6,25	0,0449	0,0427	0,0323	0,0148	0,0067	0,0717
13	6,25	6,75	0,0478	0,0443	0,0353	0,0162	0,0073	0,0760
14	6,75	7,25	0,0505	0,0457	0,0380	0,0175	0,0079	0,0802
15	7,25	7,75	0,0534	0,0471	0,0408	0,0188	0,0085	0,0844
16	7,75	8,25	0,0557	0,0482	0,0429	0,0197	0,0089	0,0878
17	8,25	8,75	0,0578	0,0493	0,0450	0,0207	0,0094	0,0910
18	8,75	9,25	0,0608	0,0508	0,0478	0,0220	0,0099	0,0955
19	9,25	9,75	0,0640	0,0524	0,0509	0,0234	0,0106	0,1003
20	9,75	10,25	0,0663	0,0535	0,0530	0,0244	0,0110	0,1037
21	10,25	10,75	0,0697	0,0551	0,0562	0,0259	0,0117	0,1088
22	10,75	11,25	0,0725	0,0565	0,0588	0,0270	0,0122	0,1129
23	11,25	11,75	0,0750	0,0577	0,0611	0,0281	0,0127	0,1165
24	11,75	12,25	0,0773	0,0588	0,0632	0,0291	0,0132	0,1200
25	12,25	12,75	0,0810	0,0606	0,0666	0,0306	0,0138	0,1255
26	12,75	13,25	0,0844	0,0622	0,0697	0,0321	0,0145	0,1306
27	13,25	13,75	0,0882	0,0639	0,0731	0,0336	0,0152	0,1361
28	13,75	14,25	0,0904	0,0650	0,0751	0,0345	0,0156	0,1394
29	14,25	14,75	0,0897	0,0647	0,0744	0,0342	0,0155	0,1384
30	14,75	15,25	0,0906	0,0651	0,0753	0,0346	0,0157	0,1398

References

[1] Wagner R.: "Accounting for the speed shear in wind turbine power performance measurement", [2010], Risø-PhD-58(EN), ISSN: 1095-4244 (*http://dx.doi.org/10.1002/we.509*), vol: 14, issue: 8, pages: 993-1004, 2011.

[2] Wagner R., Pedersen T.F., Courtney M., Antoniou I., Davoust S., Rivera R.L.: "Power curve measurement with a nacelle mounted lidar", [2014], Wind Energy, Vol: 17, issue: 9, pages 1441–1453 (*http://dx.doi.org/10.1002/we.1643*).

[3] Peña A. et al.: "Remote Sensing for Wind Energy", [2013], PhD remote sensing summer school compendium, DTU Wind Energy-E-Report-0029(EN).

[4] Eecen P.J., Wagenaar J.W., Stefanatos N., Pedersen T.F., Wagner R., Hansen K.S.: "Final report UPWIND 1A2 metrology", [2011], ECN-E-11-013.

[5] Vasiljevic N., Courtney M., Mann J.: "A time-space synchronization of coherent Doppler scanning lidars for 3D measurements of wind fields.", [2014], Ph.D. thesis, DTU Wind Energy PhD no. 0027(EN).

[6] JCGM 200:2012: "International Vocabulary of Metrology – Basic and General Concepts and Associated Terms" (VIM 3rd edition), (*http://www.bipm.org/en/publications/guides/vim.html*).

[7] JCGM 100:2008: "Evaluation of measurement data – Guide to the expression of uncertainty in measurement" (GUM), (*http://www.bipm.org/en/publications/guides/*).

[8] Gottschall J., Courtney M.: "Verification test for three WindCube WLS7 LiDARs at the Høvsøre test site", [2010], Roskilde: Danmarks Tekniske Universitet, Risø Nationallaboratoriet for Bæredygtig Energi, Risø-R-1732(EN).

[9] Borraccino A., Courtney M., Wagner R., Boquet M.: "Calibration report for Avent 5-beam demonstrator lidar", [2015], DTU Wind Energy E-0087.

[10] Borraccino A., Courtney M., Wagner R., Harris M., Slinger C.: "Calibration report for ZephIR Dual Mode lidar (unit 351)", [2015], DTU Wind Energy E-0088.

[11] Wagner R., Sathe A., Mann J. and Courtney M.: "Vector or scalar averaging for lidar 10 minute wind speed measurements", ISARS 2014.

[12] IEC 61400-12-1: Draft CDV, 30 April 2014, "Power performance measurements of electricity producing wind turbines".

[13] Courtney M.: “Calibrating nacelle lidars”, [2013], DTU Wind Energy E-0020(EN).

[14] JCGM 101:2008: “Evaluation of measurement data – Supplement 1 to the Guide to the expresssion of uncertainty in measurement – Propagation of distributions using a Monte-Carlo method, (*http://www.bipm.org/en/publications/guides/*).

[15] J. Gottschall, M. S. Courtney, R. Wagner, H. E. Jørgensen, I. Antoniou: “Lidar profilers in the context of wind energy – a verification procedure for traceable measurements”, The UpWind Special Issue, Volume 15, Issue 1, pages 147–159, January 2012 (*http://dx.doi.org/10.1002/we.518*).

[16] Lidar Special Issue: The UpWind Special Issue Volume 15, Issue 1, pages 147–159, January 2012.